

The Peano software—parallel, automaton-based, dynamically adaptive grid traversals

Tobias Weinzierl *

February 12, 2023

Abstract

We discuss the design decisions, design alternatives and rationale behind the third generation of Peano, a framework for dynamically adaptive Cartesian meshes derived from spacetrees. Peano ties the mesh traversal to the mesh storage and supports only one element-wise traversal order resulting from space-filling curves. The user is not free to choose a traversal order herself. The traversal can exploit regular grid subregions and shared memory as well as distributed memory systems with almost no modifications to a serial application code. Relying on a formalism of the software design at hands of two interacting automata—one automaton for the multiscale grid traversal and one for the application-specific algorithmic steps—we discuss the chosen callback-based programming paradigm, supported application types and the two data storage schemes realised, before we detail high-performance computing aspects and lessons learned. Special emphasis is put on observations regarding the used programming and algorithmic concepts. This transforms our report from a “one way to implement things” code description into a generic alternatives and rationale summary for some design decisions to be made for any tree-based adaptive mesh refinement software.

1 Introduction

Dynamically adaptive grids are mortar and catalyst of mesh-based scientific computing and thus important to a large range of scientific and engineering applications. They enable scientists and engineers to solve problems with high accuracy as they invest grid entities and computational effort where they pay off most. Naturally, these regions may change over time for time-dependent problems and may change throughout a solve process due to error estimators. Since the design of meshing software for dynamically adaptive grids has to support a magnitude of advanced algorithmic building blocks such as discretisation, refinement criteria, solver steps or visualisation it is non-trivial. It has to facilitate functional diversity and be accessible. At the same time, mesh storage, administration and processing have to meet efficiency and concurrency requirements of high-performance computing (HPC). One specific yet popular meshing paradigm that tries to meet these criteria and is subject of study here are spacetrees which generalise quadtrees and octrees. They yield adaptive Cartesian grids [18, 24, 30, 35, 40, 47, 48, 53, 56].

This paper orbits around the spacetree software Peano [61] that is available in its third generation. The first generation is a set of proof-of-concept codes tackling various challenges with different core code routines ([16, 42], e.g.). As second generation fuses these concepts into one code base made primarily for CFD-type applications though some generic software rationale are reported ([14, 15, 59, 62] and others). The third generation is a complete rewrite that focuses on an abstraction from any application, offers different memory organisation schemes and emphasises scalability. Our objective is two-fold: On the one hand, we want to present this third generation of the software as well as the underlying rationale and, thus, sketch its potential. While Peano is used as workhorse for our own projects ([5, 22, 46, 50, 58, 60, 63], e.g.), making it freely available allows other groups to benefit from the

*Department of Computer Science, Durham University, UK (tobias.weinzierl@durham.ac.uk)

development effort, too. For this, however, its design philosophy has to be described explicitly and academics have hence to be enabled to assess whether it suits particular needs and where certain design decisions make it inferior or superior to other codes. On the other hand, we want to identify and outline design and realisation patterns [25] for tree-based adaptive mesh refinement (AMR). Given the popularity of this meshing paradigm, our manuscript brings together and compares fundamental decisions to be made by any developer. Many of these comparisons and classifications have, to the best of our knowledge, not been done before in a concentrated effort.

While we work application-generic, we do not strive for the flexibility and diversity along the lines of other solutions such as [1, 8, 10, 18, 23, 48, 55] or others. Our approach ties the mesh traversal and programming model to the mesh structure: the user is not allowed to navigate through the grid freely. Instead, the grid traversal, i.e. the sequence in which grid entities are processed, is prescribed. This poses a restriction that may force algorithms to be redesigned, but it allows developers to focus on the question which algorithmic steps are mapped onto the processing of which grid entity (vertex or cell, e.g.) and which temporal and data dependencies between these steps exist. How the processing is realised is hidden. This picks up recent trends in task-based computing and has successfully been used in various spacetime and non-spacetime codes such as [43, 57]. A minimalist set of constraints on what to do with which grid parts and which partial orders allows us to tune the grid traversal. It further enables us to hide concurrent execution from the application codes, and it is one goal of the manuscript to highlight how such a restrictive programming model interacts with other well-known concepts such as spacetime linearisation based upon space-filling curves [53], various discretisation and data modelling choices, persistent data storage, domain decomposition and task processing. Since the traversal invokes user-defined operations and disallows users to control the traversal, our programming paradigm can be summarised by the Hollywood principle: Don’t call us, we call you [54].

A discussion of the programming model requires us to uncover and categorise the underlying design choices made w.r.t. data structures, ordering and access. Other choices would have been possible, so a description of the chosen approaches and the motivation is of use to other spacetime code developers facing similar challenges. Total linearisation of the tree through space-filling curves (SFCs), e.g., enables us to encode the grid data and adjacency with minimal memory and to stream it continuously through the processor. Holding a tree as stream rather than a pointer data structure is a popular technique and, thus, can be called a design pattern [25]. Our manuscript applies the well-known linearisation idea to multilevel grids and details the relation to depth-first (DFS) and breadth-first (BFS) searches. Depth-first linearisation yields vertically integrated [2] grid traversals—multiple levels are processed “simultaneously” data streaming—which yield excellent memory access characteristics through data accesses with oblivious spatial and temporal access locality [38], while most tree codes focus on the handling of the finest tessellation resolutions only. We detail from hereon further design decisions, notably the embedding or linking of application data with the tree structure (our results clarify that a decision which variant is superior depends on the data cardinality per grid entity), variants of tree traversal orders and their concurrency (while DFS yields vertically integrated traversals, it lacks obvious concurrency for traditional stencil codes and we thus derive a hybrid of DFS and BFS) and the decomposition of multilevel tree data over multiple compute ranks. Our latter avoids, different to other published approaches, the replication of coarse resolution data.

The paper is organized as follows: We start from a brief introduction of the grid data structure and revise the two grid enumeration schemes we rely on. The main part of the manuscript starts from a description of our callback-based programming model (Section 3). This allows us to clarify which classes of applications are supported by the code as well as application limitations. In Section 4, we review some data storage paradigms for spacetimes and classify the two storage variants offered by Peano: stream- and heap-based persistency. Three sections are dedicated to a discussion of memory movement and administration minimisation (Section 5) as well as the supported distributed (Section 7) and shared memory (Section 6) parallelisation. Special emphasis here is put on the interplay of dependencies with spacetime traversal strategies as well as the programming interface. Notably, we discuss two competing multiscale data splitting strategies, synchronisation-avoiding application interfaces and a

constraint technique that can guide a task-based parallelization though we never set up any task graph explicitly. Some experiments highlight properties of the proposed realisation ideas before an outlook closes the discussion.

2 Spacetree definition and enumeration paradigms

This paper stands on the shoulders of spacetrees. The computational domain is suitably scaled and dilated to fit into a unit hypercube of dimension d . All ingredients introduced in this paper as well as the underlying software work for any dimension $d \geq 2$. We cut the hypercube into k equidistant slices along each coordinate axis and end up with k^d small cubes. They form a Cartesian grid while the cut process describes a relation $\sqsubseteq_{child\ of}$ between the newly generated children and their parent cube. It yields an embedding of the finer into the coarser grid. Our software uses $k = 3$. Most concepts however work for any $k \geq 2$. We continue recursively yet independently for each new cell and end up with a set of cubes \mathcal{T} , where the tree leaves, i.e. the cells not refined further, span an adaptive Cartesian grid. The parent-child relation $\sqsubseteq_{child\ of}$ or its inverse, respectively, induce a hierarchy on \mathcal{T} . It renders the data structure into a tree. The overall construction process yields a cascade of ragged Cartesian grids embedded into each other. Applications requiring only the finest tessellation ignore the coarser levels, while geometric multigrid algorithms for example benefit from the nested grids.

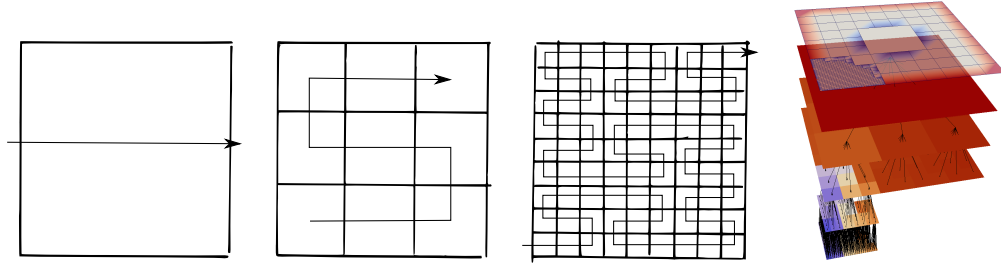


Figure 1: We embed the computational domain into a square (left). The Peano SFC motif (2nd from left) induces an ordering on a Cartesian grid (next) that results from successive refinement starting from the square (left). Illustration from [59]. The sequence depicts three regular grids $\Omega_{h,0}$, $\Omega_{h,1}$ and $\Omega_{h,2}$ which can be embedded into each other. The construction of an adaptive Cartesian grid (top right) yields a spacetree (below; from [60]). Its arising adaptive grid (top) can be read as union over all the ragged regular Cartesian grids of different resolution levels below.

Two classic enumerations of \mathcal{T} follow depth-first search (DFS) and breadth-first search (BFS). Yet, $\sqsubseteq_{child\ of}$ plus DFS and BFS remain partial orders as long as no enumeration is defined on the children of the refined cells. If we use one leitmotif for all parent-children relations, we end up with a space-filling curve (SFC) [4]. If properly equipped with rotations and mirroring, the leitmotif yields the Hilbert or Lebesgue curve for $k = 2$ or the Peano curve for $k = 3$. In our code base, we rely on the Peano curve (Figure 2) which motivates our choice of three-partitioning $k = 3$.

Observation 1. Tree and grid language for spacetrees are equivalent once we read an adaptive Cartesian grid as composite of ragged regular Cartesian grids.

Let the level ℓ of a tree's node equal the length of the path to the root of the tree, i.e. the original bounding box. The nodes of one level span a grid

$$\begin{aligned}\Omega_{h,\ell} &= \{c \in \mathcal{T} : level(c) = \ell\} && \text{with the tessellation} \\ \Omega_h &= \bigcup_{\ell} \Omega_{h,\ell}.\end{aligned}$$

Design decision 1. Cells and vertices are made unique through their position and space plus the level. Thus, multiple vertices may coincide spatially but ‘live’ on different levels.

Our approach offers complete level grids $\Omega_{h,\ell}$ and thus permits applications to hold data on each level separately. If an application exploits solely the finest grid Ω_h , vertices and cells are held redundantly and the design decision imposes an overhead. The overhead is bounded by a factor of $\sum_{\ell=0}^{\infty} \left(\frac{1}{3^d}\right)^\ell = \frac{1}{1-3^{-d}}$. Given our multilevel grid representation, we define the term *hanging vertex* in a multilevel sense, too: Most vertices of level ℓ have 2^d adjacent cells on the same level. Some vertices have fewer adjacent cells. They are hanging. Multiple hanging vertices may coincide.

Any SFC-based DFS or BFS ordering linearises the spacetree [53]. It enumerates all cells of the tree within the multiscale cascade. Peano’s core routines never use this enumeration explicitly. Instead, the enumeration orders all data structures used and thus implicitly is exploited. Yet, one data administration approach built on top of the core routines uses explicit numbering.

Within the total DFS order, cell numbers (identifiers) can be derived from the whole path from the root to any cell. The root has entry 0. Children of a refined node inherit the node’s identifier and append an number along the SFC—similar to adding additional digits after the comma if numbers were taken from $[0, 1[$. This way, it is possible to derive a cell’s position and size from its identifier, and to search the linearisation of neighbouring cells. The code formalism is equivalent to a formalisation of a recursive function running DFS through the tree: Each call stack entry then implicitly encodes one edge within the tree graph from the spacetree’s root to the current spacetree node. For a plain, continuous numbering of cells along the natural numbers this is not possible. Efficient numbering stores each cell identifier with a fixed number of bits—it constrains the tree depth—to fit them into a byte, e.g. DFS and BFS yield the same cell ordering if an algorithm solely works with Ω_h and neglects/omits coarse levels.

Design decision 2. We use tripartitioning instead of the predominant bipartitioning, and we use the Peano space-filling curve.

From an application’s point of view bi- and tripartitioning both come along with pros and cons. Aggressive $k = 3$ coarsening can pose a challenge to geometric multigrid algorithms, e.g., if a too large spectrum of solution modes is thrown away per coarsening step. In return, fine grid cell centres coincide with coarse ones for tripartitioning. This simplifies the coding of cell-centred discretisations. Another pro/con pair is the transition from one resolution h into another resolution $\hat{h} > h$ if 2:1-balancing is enforced: Our tri-partitioning creates a denser communication/data-exchange pattern than bipartitioning. In return, very fine resolutions h do not spread out that significantly into coarser regions with \hat{h} . Different considerations might arise for different applications.

While Hilbert and Peano yield face-connected DFS enumerations (see [31] and citations therein), i.e. any two subsequent cells along the SFC enumeration share one face, only Peano and Lebesgue are straightforward to extend from $d = 2$ to $d \geq 3$. Lebesgue uses a tensor-product approach, Peano extends its motif from d into dimension $d + 1$ by mirroring the d motif once, appending it along the dimension $d + 1$, and then appending on top the original motif again. As we stick to Peano, our code base supports any $d \geq 2$ though it quickly runs into the curse of dimensionality [12].

3 Spacetree application programming interface

AMR code interfaces can be classified along various metrics. We use two. Both assume that the most important operation on an AMR grid is to run over all entities. An interface either can permit the user code to arbitrarily navigate through the spacetree, or a code can prescribe the traversal order of the grid entities. Orthogonal to this decision, a user interface has to define which data the user is allowed to read and write. Strict element-wise traversals allow a code to access solely the cell data itself plus data of its adjacent vertices while they march through the grid. The other extreme of a cell-based API allows an application to read and

Table 1: A classification of spacetree user interfaces at hands of two orthogonal metrics.

	restrictive, constrained (cell-wise) data access	read and write of (non-local) grid data (RAM)
prescribed grid traversal order	Peano	Examples are deal.II or Dune (with user-defined large grid overlaps) if solely iterators are used. Yet, they allow users to navigate through the grid starting from a iterator position ...
user controls grid run-through order	p4est, e.g., supports arbitrary run-through orders while its ghost layer of width one constrains/localises data access. If users use solely p4est's iterators, the code fits into the rubric above.	...or to fuse/nest multiple iterators into each other. The exact classification of both examples depends on how they are used configured (which underlying Dune grid is used, e.g.).

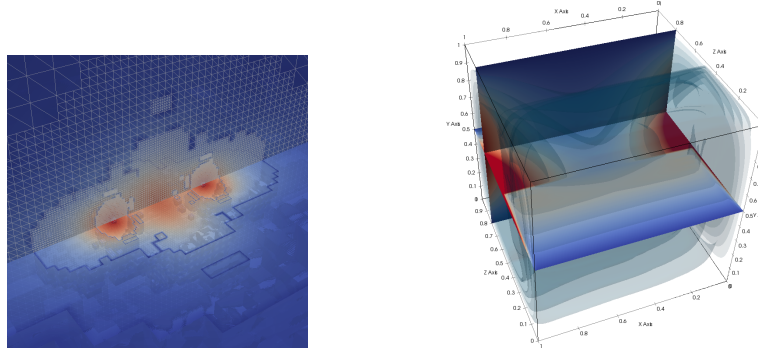


Figure 2: Left: Studies on the stability of Deuterium described by cascades of Helmholtz equations (illustration from [46]) which are solved by a low-order, complex-valued additive multigrid solver. Right: Studies on the robustness and cost of multiplicative geometric-algebraic multigrid for convection-diffusion equations (illustration from [58]).

write any data transitively associated to a cell: A code can process adjacent vertices of a cell, or any neighbouring cell associated through a face, or adjacent vertices of the neighbours, and so forth. The latter scheme supports, from the traversal's point of view, random access to the memory (RAM).

Design decision 3. Peano sticks to a strict element-wise multiscale tree traversal. All cells of each tree level are processed per grid sweep. The process order is determined by the tree traversal code. The user has no influence on this order and has to program agnostic of it. However, many temporal constraints are guaranteed, i.e. there is a partial order on the traversal's transitions. At any time solely cell data, the vertices adjacent to a cell, the cell's parent plus the adjacent vertices of the parent are exposed to the application code.

A restrictive programming model where the user is not in control of the access order allows us to hide how the data is held and maintained. It is thus our method of choice for a separation-of-concerns software architecture.

3.1 Supported application types

Different applications fit to our strict element-wise traversal. We detail some applications in the appendix and summarise the key characteristics here. Naturally, any stencil that decomposes additively over 2^d cells arranged in a cube can be realised. d -linear finite element codes (Figure 2) fall into this class as well as low order finite volume and finite difference schemes. We may assemble system matrices explicitly through PETSc [6], e.g., or evaluate

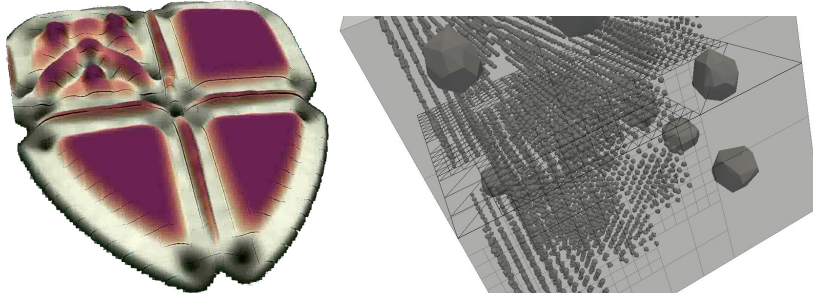


Figure 3: Left: Snapshot of a shallow water Finite Volumes solver which is applied to an initial water height profile initialised through the Durham code of arms. Each spacetree cell here hosts a patch of Finite Volumes (illustration from [60]). Right: Snapshot of a Discrete Element code where rigid particles are embedded into the Peano grid.

matrix-vector products matrix-freely, i.e. without assembly, throughout the grid traversal. Arbitrary adaptivity can be supported recursively by writing two-level interaction operations. As Peano holds all grid levels, also different stencil types of even PDEs can be hosted by different resolutions.

A spacetree cell can host a whole patch of unknowns rather than only single unknowns (Figure 3). The same concept allows us to host higher order shape functions. In this context, it is reasonable to weaken the notion of element-wisely. If we augment, similar to [35], a vertex by pointers to its 2^d adjacent cells, we can construct the inverse of the directed connectivity graph constructed by the spacetree:

Design decision 4. By default, Peano offers strict element-wise multilevel data access. Yet, we allow to weaken these data access permissions: At the price of 2^d pointers per vertex, we make each vertex point to its adjacent cell data.

This additional adjacency information is maintained, also for dynamically adaptive grids, by the traversal code: There is memory overhead to hold adjacency properties that allow us to weaken the strictness of cell-wisely. There is no additional algorithmic cost as all links, also for hanging vertices, are kept consistent on-the-fly. Patch-based codes (block-structured AMR) can either befill ghost layers or make a patch interact directly with neighbour patches [60]. If we embed $n \times n$ or $n \times n \times n$ or, in general, n^d patches into each cell, we can through the inverse adjacency information equip each patch with a ghost layer of a width of up to n .

Besides low order ansatz spaces and patches, higher order discretisations fit to the traversal as long as their support is localised. Classic Discontinuous Galerkin where the shape function support covers solely one cell yield admissible stencils. Here, multiple degrees of freedom have to be assigned to vertices or edges—edge unknowns always can be mapped onto vertex locations which implies that solely vertices have to be kept persistent from a data structure point of view—or degree of freedoms have to be stored within the cell. Higher order approaches with increased global smoothness are more difficult to realise: B-spline shapes spanning multiple cells for example seem to misfit the element-wise concept. Yet, we can, for example, rely on n^d patch data structures with a ghost layer of width n carrying higher order shape functions such as B-splines of order $2n - 1$. Support overlaps from one spline with others then can be evaluated.

Particle-grid formalisms such as Particle-In-Cell (PIC) fit to our concept as long as the particle-grid interactions do not span more than one cell: If particles fall into a cell, they may interact solely with the 2^d adjacent vertices of this cell if they are held within the cell. Alternatively, we can assign each particle to its closest vertex and thus store them in a dual tree grid [63]. This facilitates wider interaction areas.

Particle-particle interactions are straightforward to realise if we rely on the aforementioned neighbour cell links [21] and if the interaction radius fits the mesh width. Again, particles can live on different spacetree levels (Figure 3). Moving them through various levels facilitates tunnelling where particles move more than one cell per time step [63].

Algorithm 1 Depth-first traversal of spacetree. It is invoked on the trees root and is passed the linearised tree as S_{in} . It yields the output stream S_{out} subject to dynamic grid refinement and coarsening which is used for the next traversal. S is the traversal automaton state encoding the space-filling curve (level, orientation, ...) and the cell's position and size h .

```

1: function TRAVERSE( $S_{in}, S_{out}, S$ )
2:    $currentCell \leftarrow pop(S_{in})$ 
3:   for adjacent vertices  $v$  of  $currentCell$  do
4:     if  $v$  is hanging vertex on level  $\ell$  then
5:        $createHangingVertex(v, \dots)$ 
6:     else if  $v$  used for the very first time then
7:        $v \leftarrow$  load from input stream
8:        $touchVertexFirstTime(v, \dots)$ 
9:     else
10:       $v \leftarrow$  load from temporary data container
11:    end if
12:  end for
13:   $enterCell$ 
14:  if  $currentCell$  is refined or to be refined then
15:    for  $i \in \{0, \dots, 3^d - 1\}$  along SFC( $S$ ) do                                 $\triangleright$  Meander along SFC motif
16:      TRAVERSE( $S_{in}, S_{out}, S$ )                                           $\triangleright$  Pass down mirrored, scaled and translated  $S$ 
17:    end for
18:  end if
19:   $leaveCell$ 
20:  for adjacent vertices  $v$  of  $currentCell$  do
21:    if  $v$  is hanging vertex on level  $\ell$  then
22:       $destroyHangingVertex$ 
23:    else if  $v$  used for the very last time then
24:       $touchVertexLastTime$ 
25:      store  $v$  on output stream for next traversal
26:    else
27:      store  $v$  in temporary data container
28:    end if
29:  end for
30:  if part of grid not to be erased then
31:     $push(currentCell, S_{out})$ 
32:  end if
33: end function

```

3.2 An automaton-based traversal

As we disallow the user to navigate through the spacetree herself (Table 1), we read the multi-scale Cartesian grid traversal as a deterministic push-back automaton—the formal equivalent to a recursive function—that reads the tree structure from an input stream while adaptivity criteria insert or remove elements. It runs from cell to cell (Algorithm 1).

Without the optimizations from Section 6, we make the automaton run through the tree along a modified DFS. Such a convention facilitates a memory-efficient realisation of the automaton (cmp. Section 4) and makes the automaton run through each spacetree cell twice: once throughout steps the down, once when it backtracks bottom-up. This equals an element-wise multiscale adaptive Cartesian grid traversal which is formalised by a sequence of transitions such as ‘move from one cell into another cell’. In our code, these transitions act as plug-in points for the application-specific functions (compute kernels) [43]. We refer to them as *events* (Table 2). Events are defined on cells, vertices or traversal start and end.

Design decision 5. Peano does not impose any balancing condition, i.e. each hyperface in the grid may host an arbitrary number of hanging vertices [33, 48, 53]. However, balancing can be enforced by the user if favoured by the application domain. There’s no tailored/optimised handling realised in the code so far to avoid rippling [53], i.e. rippling has to be picked up by the user through additional grid sweeps.

A user writes routines that are invoked on grid entities through the transitions. The routines’ semantics may depend on a state. Such a system can be read as a combination of two automata (Figure 3.2): One runs through the spacetree. Its transitions trigger stimuli that feed the other automaton implementing the solver’s behaviour as reaction. Stimuli comprise both automaton properties such as position in space, level, grid statistics (such as the total

Table 2: Table of events defined by Peano that act as plug-in points for the application.

Event	Semantics
<code>beginIteration</code>	Is called once per tree traversal prior to any other event.
<code>endIteration</code>	Is called once per tree traversal in the very end.
<code>createVertex</code>	Creational event [25] that allows proper intialisation of vertices. Is invoked only once per vertex if the grid is refined by the traversal automaton.
<code>destroyVertex</code>	Counterpart of <code>createVertex</code> invoked just before the memory of a vertex is released. Is invoked by the traversal automaton once before it erases parts of the spacetree.
<code>createHangingVertex</code>	Hanging vertices are never held persistently but (re-)created on-the-fly whenever they are required, i.e. whenever an adjacent cell on the respective level is traversed. This implies that a hanging vertex might be created up to $2^d - 1$ times.
<code>destroyHangingVertex</code>	Counterpart of <code>createHangingVertex</code> .
<code>createCell</code>	Creational event for cells.
<code>destroyCell</code>	Counterpart of <code>createCell</code> .
<code>touchVertexFirstTime</code>	Event invoked on a vertex once per traversal just before it is used for the very first time.
<code>touchVertexLastTime</code>	Event invoked for a vertex after all adjacent cells have been traversed.
<code>enterCell</code>	Whenever the traversal automaton enters a spacetree cell, it invokes an <code>enterCell</code> event.
<code>leaveCell</code>	Counterpart of <code>enterCell</code> that is invoked throughout the automaton's backtracking.
<code>descend</code>	Variant of <code>enterCell</code> that is offered to simplify multigrid algorithms. Passes a refined cell plus its adjacent vertices to the application-specific code as well as all 3^d child cells and their 4^d vertices.
<code>ascend</code>	Counterpart of <code>descend</code> .

number of vertices) and the data associated to the event. Data circumscribes vertex attributes for vertex-based events, cell attributes plus all attributes of adjacent vertices for cell-based events, and always the same type of data associated to the next coarser level, i.e. to the parent grid entity. The latter facilitates the realisation of multiscale applications. Level and spatial properties are held within the automaton state and thus are not stored within the vertices and cells. This is memory efficient. The event-based programming model forces the user to express all algorithms in local operations (element-wisely) as well as two-grid kernels. The application code may express the wish to refine or coarsen the grid to the traversal through the return value of the events.

Let $a, b \in \mathcal{T}$ with $a \sqsubseteq_{child} b$. Further, v_a, v_b are vertices adjacent to a or b , respectively. While the processing order of cells and vertices is hidden, all applications can rely on the invariants

$$\begin{aligned}
\text{touchVertexFirstTime}(v_b) &\sqsubseteq_{pre} \text{touchVertexFirstTime}(v_a), \\
\text{touchVertexFirstTime}(v_b) &\sqsubseteq_{pre} \text{enterCell}(b), \\
&\text{enterCell}(b) \sqsubseteq_{pre} \text{enterCell}(a), \\
&\text{enterCell}(a) \sqsubseteq_{pre} \text{leaveCell}(a), \\
&\text{leaveCell}(a) \sqsubseteq_{pre} \text{leaveCell}(b), \\
&\text{leaveCell}(a) \sqsubseteq_{pre} \text{touchVertexLastTime}(v_a), \\
\text{touchVertexLastTime}(v_a) &\sqsubseteq_{pre} \text{touchVertexLastTime}(v_b).
\end{aligned} \tag{1}$$

\sqsubseteq_{pre} is a temporal relation. It identifies which event is invoked prior to another event. It is easy to verify that DFS and BFS both suit (1).

Design decision 6. We allow the application automaton to flag operations from Table 2 as empty. They then are automatically skipped and thus removed from (1).

Observation 2. In the context of trees in object-oriented languages, our inversion of control—the application kernels do not determine how the data structures are processed—

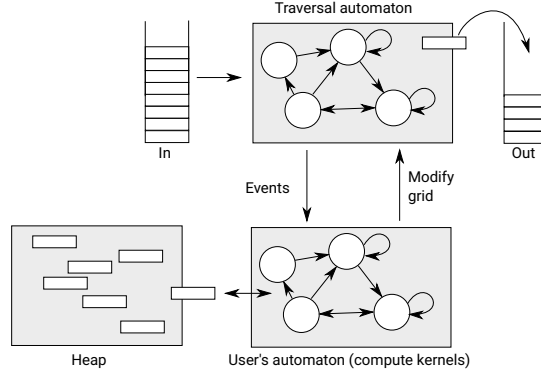


Figure 4: The traversal automaton runs through the grid (top) reading in streams and piping out streams. Each transition triggers kernels in the application-specific automaton (bottom) that may use or may not use heap data.

can be read as a composite pattern in combination with a visitor pattern [25]. In the context of finite element (FEM) solvers, this paradigm is used by various codes [18, 43, 57]. In the context of general programming, it mirrors higher-order functional programming where the application’s function set is passed to the traversal function.

We favour to call the programming pattern Hollywood principle [54]: Don’t call us, we call you. The user’s implementation is unaware of when events are invoked—though the constraints (1) hold—it is unaware where events are invoked in a distributed environment, and it is unaware of any other events invoked concurrently.

3.3 Limitations of the approach

Our API poses limitations. First, the grid’s structuredness does not offer the flexibility of unstructured meshes though users can weaken the structuredness by embedding unstructured/point data into the spacetree cells. Second, the hiding of traversal details makes the code not a black-box library that can be used within any code base through few library invocations. It requires users to break down their algorithm’s workflow into events and dependencies first. The “loss of control” might require algorithm designers to rethink code snippets and algorithmic realisations. Finally, a very strict element-wise mindset is not the standard mindset of many application developers. This steepens the learning curve.

4 Persistency model and data management

How to store the spacetree is an important design decision for a software. Also, we have to clarify how to hold data associated to the grid.

4.1 Spacetree storage schemes

To hold the spacetree, we distinguish two paradigms: The tree either is mapped onto a graph—typically structures/classes with pointers—or it is held linearised. Hybrids exist. Graph-based approaches are flexible but suffer from pointer overhead. Furthermore, the tree records scatter in memory and induce non-local memory accesses for a traversal code once the grid is subject to strong dynamic adaptivity. This may cause poor memory usage profiles. Yet, a spacetree mapped onto a graph data structure still yields a lower memory footprint than arbitrary unstructured grids, as associativity between cells is encoded in the tree relations: a cell neighbour either is a sibling, or a particular child of the sibling of the parent node, and so forth. We note that some graph approaches exploit structuredness, i.e. combine the graph with linearisation: siblings can be stored as one block [24, 35] or regular grids are used on

certain grid levels [23] and thus increase data access locality while they reduce the memory footprint.

As alternative to the graph, we may hold the spacetree in a stream. This stream holds all cells of the spacetree according to a total order on \mathcal{T} . A natural approach stores the DFS plus SFC code within the stream. As the code comprises the cell’s level plus position, lookups for neighbours within the stream are efficient—a neighbour’s code can directly be computed by bit-wise index manipulations.

Observation 3. Linearised spacetrees are superior to graph-based data structures, i.e. structs connected via pointers, in terms of memory as they only require one code (identifier) to be stored per cell.

As we forbid control over the traversal order in our code and stick to a DFS/SFC combination, we can implement the tree traversal as recursive function (Algorithm 1). It is a push-back automaton relying on the system’s call stack. The automaton knows at any time its level and position and thus solely has to know from an input linearisation whether to recurse further or not. No maximum tree depth constraints are imposed while two bits per cell (unrefined, refined, to be refined, to be erased) are sufficient to store all the dynamic adaptivity information [62]. For static adaptive grids, one bit is sufficient. In Algorithm 1, these bits are encoded within S_{in} .

Design decision 7. Peano linearises the tree along the Peano SFC. It sticks to a DFS and the traversal thus reads in the spacetree as bit stream.

To support arbitrary adaptivity, it is advantageous to make the automaton read one bit stream and output another stream that acts as input to the subsequent traversal. We hence avoid data movements due to insertion and deletion while the stream read/writes are advantageous in terms of memory access characteristics. They yield high temporal and spatial data access locality [38]. Yet, for reasonably structured grids we abandon the strict linearisation (Section 5).

4.2 Application data management

Automaton-based spacetree traversals do not prescribe how the actual application records are held. Besides graph-based descriptions—spacetree entities hold pointers to cell or vertex properties—two storage strategies candidate. On the one hand, spacetrees can be both a technique to encode the grid structure and a container for the data itself. On each and every level, the user assigns data to vertices and cells, and the stream of the spacetree is enriched with this application-specific data. The spacetree then acts as both organisational and compute data structure. On the other hand, we can rely on a heap. All data are stored within a (hash) map. The cell’s DFS/SFC identifier contained in the automaton state is a natural candidate to provide a key to this hash map. Vertex keys can be derived from the cell codes. Alternatively, we may use pointers directly [18]. With a semantic separation of the tree/grid data container from an application container, the realisation resembles (author?) [7]. However, our implementations are originally inspired by (author?) [29, 30]. If the grid does not change too frequently, it is, as a variation of the hash storage, convenient to flatten also the application data along the spacetree linearisation and hold it as one big chunk of data accessed along the SFC. This is particularly interesting for hardware suffering from indirect and scattered memory access. We omit this variant as we assume that our grid changes in each and every grid sweep, and point out that such data flattening/reordering is subject of discussion next.

Design decision 8. Both data storage strategies—embedding data into the spacetree and holding it in a separate hash map—are available in Peano: We refer to them as stack-based or heap-based data storage.

Both variants come along with pros and cons. If we embed PDE-specific data into the read/write streams, data associated to the respective cell as well as vertex data are immediately available to the automaton. Records associated to the spacetree cells are directly interwoven with the spacetree’s bitstream. Records associated to the spacetree vertices are

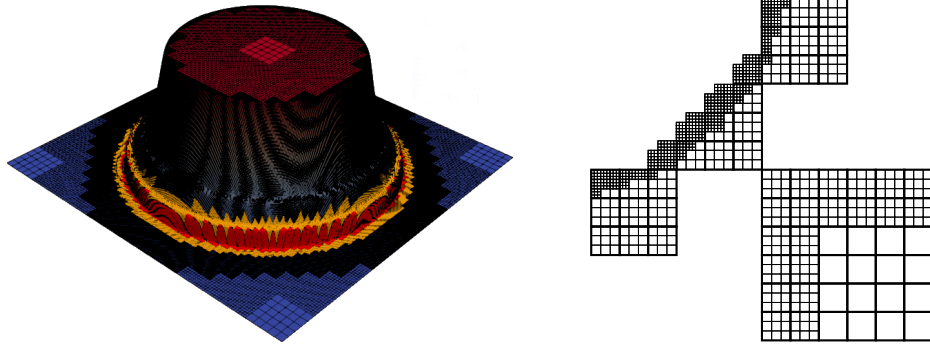


Figure 5: Left: Euler equation simulation of a point shock from the ExaHyPE project [5]. Right: Illustration of the skeleton grid of the bottom corner from the left simulation, i.e. the grid that is held as a tree if all regular subtrees of dimension 9×9 or bigger are held as separate regular grids.

held in a separate stream. It is ordered along `touchVertexFirstTime`. We show in (author?) [59, 62] that we can write out the vertex data as stream following `touchVertexLastTime` and use this stream as input the subsequent iteration even if the grid is dynamically adaptive. Throughout the grid traversal, vertices temporarily have to be stored on stacks. The stacks serve temporary data containers in Algorithm 1. $2 \cdot d$ such stacks are required and their maximum size is bounded by the spacetime depth. The number of stacks is fixed, small, and their size is small, too. Cell-vertex associativity is encoded in the grid traversal automaton, i.e. the automaton knows at any time from which data container (stream or stack) to take all vertex data from and where to write vertices to before the next cell is entered. The whole scheme comes for free in terms of user source code—the automaton simply hands over references to the stacks to the user automaton—the total memory footprint is minimal and all data remains read and written in a stream/stack fashion. This yields excellent memory access characteristics [15, 42, 46, 59, 62, 63].

The method falls short if the data cardinality per vertex and cell varies—our cell or vertex stack entries all have to have the same byte count—or if the data per cell/vertex is massive and thus moving it from one stack to another is expensive. In this case, heap-based storage is advantageous though it requires additional coding, induces hash bookkeeping overhead and may introduce scattered data with non-uniform data access cost. Yet, efficient hash codes exist [47, 56]. Notably DFS/SFC codes yield high quality hash codes or preimages to a hash function due to their Hölder continuity [4, 16, 26, 29, 30, 32].

5 Reduction of tree traversal overhead

DFS tree traversals are a powerful tool to facilitate arbitrary dynamic adaptivity for meshes that change frequently. As we realise the tree’s linearisation through a recursive function, i.e. a pushback automaton, we however end up with a code that requires a certain amount of integer arithmetics and callstack administration (recursion overhead). This overhead is not negligible if (i) we study codes with low arithmetic intensity per grid entity and (ii) the user cannot mask out operations a priori. The latter feature is enabled by additional callbacks that can be used to clarify that `enterCell` for example in some algorithmic phases never is invoked on refined cells. In this case, Peano omits them automatically, and it obtains performance closer to codes that work on the fine mesh Ω_h only—though the performance gap never will be closed as our code is inherently written for multiscale.

This cost can be reduced if we embed regular subgrids (patches) into the cells [60]. Traversing Cartesian arrays is among the best-understood and cheapest traversal variants. A code with a spacetime hosting regular patches thus yields an administrative overhead that is in-between the minimalist cost of Cartesian grids and the cost of unconstrained dynamically

Table 3: One characterisation of various levels of structuredness and flexibility for locally regular adaptive grids. While the simplicity reduces form left to right, the flexibility (where are we allowed to invest grid entities) increases.

Regular grid	Cartesian	Block-structured AMR (patch-based) with logical tree topology between patches	On-the-fly block identification as realised in Peano	Pure tree codes
Globally simple, i.e. simple administration and data access		Simple per entity (block/patch)	Simple per identified block; remaining (skeleton) grid complex	No regular data accesses and simple programming (without indirect addressing, e.g.)
No adaptivity		Adaptivity constrained	No constraints on adaptive patterns	No constraints on adaptive patterns

adaptive spacetree meshes. The resulting grid layout then resembles the classic AMR grids of the first hyperbolic equation AMR codes scaling up [1]. However, a refinement criterion then is not free to adopt arbitrarily accurate to a feature anymore. It has to overlap features of interest with patches. As alternative to patches, one can temporarily or locally disallow the tree to coarsen or refine and then skip many logical checks.

Let a balanced spacetree be a tree where any path from the root to a leaf has the same length. A balanced spacetree yields a cascade of regular Cartesian grids. We therefore refer to such trees as regular spacetrees. Their BFS traversal first running from coarse to fine and then backtracking from fine to coarse combines the efficiency of regular Cartesian access with the constraints from (1). We thus identify regular subtrees within the spacetree that do no change and do not accommodate any hanging vertices—they trigger additional events—on-the-fly and to switch from the DFS event invocation on this spacetree to BFS [22].

5.1 Transformation of DFS into BFS

To find the regular subtrees we rely on an analysed tree grammar [36]. Let each spacetree cell hold a marker f with

$$\forall c \in \mathcal{T} : f(c) = \begin{cases} 0 & c \text{ is a leaf with no hanging adjacent vertices,} \\ \hat{f} & \text{if } c \text{ is refined and } \forall a \sqsubseteq_{child \text{ of } c} : \\ & f(a) = \hat{f} - 1, \text{ or} \\ \perp & \text{otherwise.} \end{cases} \quad (2)$$

Equation (2) is accompanied by some veto mechanisms overruling the outcome of (2): If refinement or grid coarsening is triggered, all markers of surrounding cells are cleared to \perp . f is an augmentation of the spacetree bit stream and can be maintained on-the-fly: we take f from the input stream for our optimisation while we concurrently redetermine its new value for the subsequent traversal. In any iteration following the identification of an $f > 1$, the traversal automaton can modify its event invocation and data processing [22, 50]: If it encounters a cell with label $f > 1$, it knows that from hereon a regular subtree of depth f is to be traversed. We know how much data for this subtree is to be read from all input streams, and we create a temporary buffer in the memory than can accommodate the whole regular subtree as a cascade of regular Cartesian grids. This buffer is befilled. Following the load, the automaton invokes all the `touchVertexFirstTime`, `enterCell`, and so forth events in a BFS order, before the tree is streamed to the stacks again. Formally, the reordering is local recursion unrolling.

If the BFS is fed a refinement or coarsening request by the application automaton, the markers in the regular subtree are set to \perp and we bookkeep the erase or refine request. It is realised in the subsequent iteration when the subtree is not treated as a regular one anymore due to the invalidated f .

5.2 Persistent regular subtrees

By default, the DFS-BFS transformation is applied locally, on-the-fly and temporarily, while we preserve the DFS/SFC input and output order on all streams. Though our approach eliminates many case checks and allows for an efficient triggering of events, it retains recursive code parts for the loads/stores from the streams to the Cartesian buffers and back.

Provided that regular subtrees remain regular, we can remove them from the tree stream and hold them as cascade of Cartesian mesh separately (Figure 5). Vertices from the regular subtree that are adjacent to the remainder of the (adaptive) grid are replicated. Prior to entering a regular subtree, these vertices are updated with the most recent vertex version from the spacetree stream. Once a subtree is processed, vertices are mirrored back. These consistency updates can be done efficiently as they affect a lower-dimensional submanifold only and as a projection of the Peano SFC onto the face of the cube spanned by the regular subtree yields a dimension-reduced Peano SFC on the face again [59, 62]. The projection yields a total order that matches the inverse of the SFC’s total order on the remaining grid’s entities [50]. Our linearised spacetree spans a holed grid, a skeleton grid, with links to regular subtrees. Though this is a pointer-linearisation hybrid, consistency data exchange all follows the SFCs through stacks.

If an application code wants to modify the grid within a regular subtree, we postpone the grid modification and first reintegrate the linearised subtree into the spacetree stream. The follow-up grid sweep then refines or coarsens. The technique follows the cluster-based AMR of (author?) [49] but combines it with (2) to identify stationary clusters on-the-fly, applies it solely to regular subtrees, and augments it by the multiresolution grid notion.

It is similar to approaches composing the AMR grid as assembly of regular patches. However, we do not start from regular patches as building blocks. Instead, we identify regular subregions on-the-fly and treat them then more efficiently than the remainder of the grid. The adaptivity of the spacetree mesh that can be constructed therefore is not restricted at all (Table 3). Regular subgrids are held separately and the linearised tree encodes only the skeleton in-between or those regions that change frequently (Figure 5). The grid is decomposed. We notice the similarity of this decomposition to a generalised variant of enclave partitioning [52] though we use our technique solely to reduce administrative overhead rather than to parallelize.

6 Shared memory concurrent traversals

Shared memory parallelisation shall be lightweight, shall not synchronise much data and enable work stealing to adopt seamlessly to changing workload. Task-based systems promise this.

Observation 4. Our event-based programming model can be casted into a task language: the user implements a fixed set of task types (event implementations), the constraint set (1) describes task dependencies, and the tree instantiates the tasks.

6.1 Dependency-based programming interface

The observation implies that we may throw any pair of traversal and user automata directly into a task management system. However, not all codes allow for a concurrent invocation of all events from (1). They impose additional constraints on the data accesses.

A matrix-free matrix-vector product for example may not allow two adjacent cells on the same level to add their residual contributions to the vertex concurrently. Red-black Gauß-Seidel-type colouring of cells with 2^d colours ensures that no vertex is accessed simultaneously in this case. Peano allows user codes to specify per event per algorithmic step which colouring would ensure on a regular Cartesian two-resolution grid that no data races occur. We support a range of colouring choices:

- A complete serialisation which is for example important to events that run IO and thus have to veto any concurrency.

Table 4: If ran on shared memory, Peano introduces two additional events.

Event	Semantics
Copy constructor	The class holding all events, i.e. the automaton, is replicated in parallel sections per thread. The copy constructor allows the user to plug into the replication.
<code>mergeWithWorkerThread</code>	If the traversal automaton leaves a grid region handled concurrently, all adapter replicates are merged into a master copy and destroyed afterwards.

- A degenerated colouring (one colour) implies that all cells or vertices, respectively, can be processed concurrently.
- 2^d colouring of cells ensures that no two cells access a shared vertex simultaneously.
- 3^d colouring on cells ensures that no two cells with the same parent cell are handled concurrently. This is useful for multiscale algorithms.
- 4^d colouring generalises this idea to vertices.
- 6^d colouring ensures that whenever two cells are handled in parallel, their parent cells do not share any vertex.
- 7^d colouring generalises this idea to vertices.

Design decision 9. We allow the user code to specify per event which concurrent data writes have to be avoided on a regular grid. It is Peano’s responsibility to schedule a well-suited parallel execution of all tasks.

For a given spacetime \mathcal{T} , the constraints (1) plus the colouring per event define a race-free task graph. While we ask the user to model colouring constraints in terms of a cascade of regular grids and hide the complexity of multicore processing of a tree, all constraints translate to the dynamically adaptive grid.

6.2 Task parallelisation without task graph assembly

Once a task graph is determined, there are two main possibilities to issue the tasks: The task graph can be assembled and handed over to a scheduler. For static grids, this can be done in a preprocessing step. For dynamically adaptive grids, it has to be done once per grid sweep, and the obtained concurrency has to make up for assembly cost. Alternatively, a grid traversal order which accommodates the task graph can be chosen: continuous chunks of grid entities within the traversal order describe independent tasks and can be in parallel, before the next chunk of grid constituents is traversed.

Design decision 10. In Peano, the traversal order follows the task dependencies and the task dependency graph is never set up explicitly.

We notice that the DFS chosen for the spacetime linearization (Algorithm 1) exhibits a poor concurrency. All cell accesses are serialized. Solely a few vertex-based events such as `touchVertexFirstTime` can be evaluated in parallel. If the user code adds a dependency between these vertices, even this negligible concurrency is eliminated. While we realise concurrent event invocations in the DFS traversal and also parallelise the automaton code itself, BFS is a better traversal for parallel for/stencil codes.

We accept the DFS’ limited concurrency in general, and use the recursion unrolling’s BFS to issue tasks in parallel if possible. The reordering of spacetime cells and the concurrent triggering of events impose bulk-synchronous programming (BSP) on the application automaton: The application normally is passed events sequentially. When the traversal automaton runs into a regular subtree, it forks the application automaton. The BFS event invocations subsequently are reordered to suit the dependencies. When the automaton leaves a regular subtree, all application automata are merged again. We reveal this by two additional events

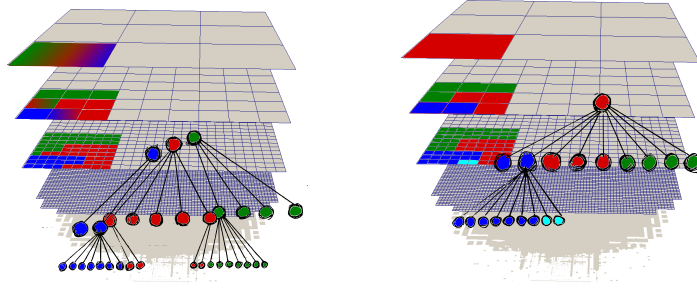


Figure 6: Bottom-up spacetree decomposition (left) vs. top-down approach (right).

(Table 4) establishing an API that hides the realisation with OpenMP or Intel’s Threading Building Blocks. They allow the application developer to focus on data dependencies and data reduction.

6.3 Limitations of the approach

BSP as currently realised in Peano does not support data access patterns where some cells depend on their neighbours or parents while other cell pairs induce no constraint. We assume homogeneous dependencies. The parallelisation kicks in for regular subgrids, while unstructured grid regions, i.e. the skeleton, the MPI domain boundaries or start and wrap-up phases of single grid traversals do not really benefit from multiple cores. If the grid changes globally per grid traversal or does not exhibit regular subregions, our approach does not exhibit lots of concurrency. Finally, we note that sophisticated multithreading exploits concurrency spanning multiple iterative sweeps. Such a blocking is not built in.

7 Tree decomposition

We discuss our non-overlapping spacetree decompositions in this section. Non-overlapping refers to the fine grid here, i.e. we assume that each fine grid cell/spacetree leaf is assigned to exactly one rank. Extensions of our techniques to overlapping decompositions are beyond scope.

We emphasise that our goal is to retain the spacetree concept in a distributed environment. Despite the parallelization, we make each rank still hold a spacetree and, thus, we allow each rank to continue to traverse its spacetree as discussed so far. The traversal logic from a serial code (Table 2) is agnostic regarding the parallelization. However, there are additional MPI-specific events.

7.1 Bottom-up and top-down tree partitioning

If the finest grid level is non-overlappingly distributed among ranks, we have to clarify which rank holds which coarser grid entities. Two options exist (Figure 6): We can either assign the responsibility for every cell on every level to a unique rank or we can replicate coarser grid levels on multiple ranks. Such a distinction is important even for codes working solely with the finest grid, as it clarifies whether individual ranks are aware of the overall spacetree decomposition or just manage local decomposition knowledge. For the actual data flow however, both tree partitioning approaches become the same if solely the fine grid Ω_h is of interest.

Spacetree replication results from a classic bottom-up scheme: We start from the adaptive fine grid and decompose its cells into chunks. From hereon, we construct each rank’s spacetree recursively: let a cell $a \in \mathcal{T}$ be held by a particular rank with $a \sqsubseteq_{child\ of} c$. Then, c is held by this rank, too. Obviously, c is replicated on several ranks if its children are replicated or distributed among several ranks. The coarsest spacetree cell is available on all ranks. Bottom-up schemes often use the term local tree for the tree held on a particular rank. The coarser

Table 5: Additional events that are available in Peano if code is compiled with MPI.

Event	Semantics
<code>mergeWithNeighbour</code>	Called for a vertex per neighbouring rank before <code>touchVertexFirstTime</code> is invoked. Passes a copy, i.e. the received replicate, from the neighbour alongside with the vertex data.
<code>prepareSendToNeighbour</code>	Counterpart of <code>mergeWithNeighbour</code> that is called per neighbouring rank after <code>touchVertexLastTime</code> to produce the copy of the vertex that is then sent away.
<code>prepareSendToWorker</code>	Plug-in point to transfer data from master to worker just before the worker's traversal is invoked.
<code>prepareSendToMaster</code>	Plug-in point to transfer data from worker to master just before the worker quits a traversal.
<code>mergeWithWorker</code>	Counterpart of <code>prepareSendToWorker</code> invoked on the worker.
<code>mergeWithMaster</code>	Counterpart of <code>prepareSendToMaster</code> invoked on the master.
<code>prepareCopyToRemoteNode</code>	Event invoked just before data is migrated to another rank due to dynamic load balancing.
<code>mergeWithRemoteDataDue-ToForkOrJoin</code>	Counterpart of <code>prepareCopyToRemoteNode</code> . Rebalancing comprises two steps: a replicate of the tree parts is created on the new remote worker and then the data is transferred through these two events to the new worker. This way, data that can be regenerated on-the-fly does not have to pass through the network.

the level the more redundant the data. This implies that (fragments of) global knowledge about the chosen domain splitting is available per subtree.

The opposite approach without data replication is a top-down splitting [59]: We assign the global spacetree root to one rank. For each $a, c \in \mathcal{T}$, $a \sqsubseteq_{\text{child of } c}$ with c associated to a rank r_1 , a is either held by this rank r_1 as well, or it is deployed to another rank r_2 that has not been employed on a coarser or the same level yet. We exempt siblings along the SFC from the latter constraint. The rule applies recursively. It introduces a logical tree topology among the compute ranks: r_2 serves as worker to a master r_1 . Whenever a child of a refined cell is assigned to another rank, this child acts as root of a remote tree. We cut out subtrees from the global spacetree.

Observation 5. The majority of spacetree codes favour, to the best of our knowledge, the partial replication with SFC cuts.

Using SFCs to obtain an appropriate initial splitting of the finest grid level is popular. SFC partitions exhibit an advantageous ratio-to-volume ratio¹ and result from a straightforward splitting of the SFC's one-dimensional preimage, i.e. the enumeration of cells. We note that SFCs also can be used for the top-down splitting as the SFC motif orders all levels: As long as any rank forks subtrees only along the SFC to other ranks, the resulting splitting is an SFC-splitting, too.

Design decision 11. Peano works with a non-replicating data layout.

Ranks in Peano are aware only of their multiscale neighbours as well as their master and worker ranks. No global information is held per rank.

7.2 Parallel tree traversal

A parallel tree traversal on replicated trees yields one automaton per rank, each traversing its local linearised tree. All start their tree traversal at the same time. Tree nodes are labelled as replicated, local or empty. Empty spacetree nodes are required if only some children of a refined node are processed locally, i.e., they are nodes purely required to complete the spacetree. As multiscale data is held redundantly, all information flow from coarser to finer grids can be realized without communication. After or throughout the backtracking, all replicated data has to be synchronized.

¹To the best of our knowledge, the good ratio is an empirical observation that can be backed-up by proofs only for regular grids where it results directly from the Hölder continuity (cf. [4, 16] and references therein).

A parallel tree traversal for the non-replicated tree yields one automaton per rank, too. However, the automata may not run in parallel right from the start since they are synchronized with each other through (1). If a child of a refined cell is assigned to a remote rank, the remote rank’s traversal automaton is triggered to start traversing ‘its’ tree by the automaton traversing the refined cell. This motivates the term worker. Throughout the bottom-up steps, an automaton in return has to wait for workers to finish prior to further backtracking. Both master-worker and master-worker communication are point-to-point communication keeping the two-grid interface between masters and workers consistent.

Algorithm 2 Blueprint of our level-wise depth-first traversal.

```

1: function TRAVERSE( $S_{in}, S_{out}, S$ )
2:   for  $i \in \{0, \dots, 3^d - 1\}$  along SFC( $S$ ) do
3:      $currentCell_i \leftarrow pop(S_{in})$  ▷ Load  $3^d$  children in one rush
4:   end for
5:   for  $i \in \{0, \dots, 3^d - 1\}$  along SFC( $S$ ) do
6:     for adjacent vertices  $v$  of  $currentCell_i$  do ▷ Load their vertices
7:       if  $v$  is hanging vertex on level  $\ell$  then
8:          $createHangingVertex(v, \dots)$ 
9:       else if  $v$  used for the very first time then
10:         $v \leftarrow$  load from input stream
11:         $touchVertexFirstTime(v, \dots)$ 
12:       else
13:         $v \leftarrow$  load from temporary data container
14:       end if
15:     end for
16:   end for
17:   for  $i \in \{0, \dots, 3^d - 1\}$  along SFC( $S$ ) do
18:     if  $currentCell_i$  is root of deployed subtree then
19:       trigger remote traversal of  $currentCell_i$  and continue
20:     else
21:        $enterCell(currentCell_i)$ 
22:     end if
23:   end for
24:   for  $i \in \{0, \dots, 3^d - 1\}$  along SFC( $S$ ) do
25:     if  $currentCell_i$  is refined or to be refined and not remote then
26:       TRAVERSE( $S_{in}, S_{out}, S$ ) ▷ Pass down mirrored, scaled and translated  $S$ 
27:     end if
28:   end for
29:   for  $i \in \{0, \dots, 3^d - 1\}$  along SFC( $S$ ) do
30:     if  $currentCell_i$  is root of deployed subtree then
31:       wait for remote traversal on  $currentCell_i$  to terminate and reduce data (if reduction enabled)
32:     else
33:        $leaveCell(currentCell_i)$ 
34:     end if
35:   end for
36:   ...
37: end function

```

DFS is problematic for parallel codes without replication unless communication is explicitly eliminated as discussed below: It is strictly sequential. Peano therefore applies one-step recursion unrolling [22, 59] on the DFS: In each refined node, the automaton reads in all children. After the k^d children are processed, they are put on the call stack and the automaton descends along the children’s order. Once all k^d recursive descends have terminated, k^d cells are taken from the call stack and the code backtracks. This is a one-step breadth-first traversal within the depth-first framework. We call it *level-wise depth-first* (Algorithm 2). It allows us to trigger remote subtree traversals before we descend locally. Though it resembles (2), it does not rely on f and is applied always; even if the tree is subject to change. Level-wise DFS is not literally a third traversal paradigm realized: It evolves from DFS through a one-step recursion unrolling, while BFS can be read as transitive hull of one-step recursion unrolling steps over DFS. Peano’s mesh traversal thus can be formalised through DFS plus one-step recursion unrolling.

The replicating scheme comes along with a higher memory overhead than the top-down splitting. There is consequently more data to keep consistent, and data exchange involves typically more than two ranks—notably on the global root of which all ranks hold a replica. The

top-down approach requires solely point-to-point data exchange and minimises data redundancy. However, top-down induces a tighter, latency-sensitive coupling [63]: data of coarse cells is propagated into finer grid resolutions which might act as coarsest resolutions to remote trees throughout the descend of the automaton. This on-the-fly information propagation has to integrate into the wake-up calls of traversal of worker ranks. Similar observations hold for the bottom-up information flow.

7.3 Data exchange

Both decomposition schemes distinguish two types of data exchange: Vertices that are adjacent to cells handled by different ranks are replicated among all ranks and are subject of horizontal data exchange [45] to keep them consistent. Vertices and cells that are held on two ranks due to a master-worker decomposition are subject of vertical data exchange.

Vertical data exchange is synchronously realized. Data is sent from the master to the worker upon the wake-up call and coarse information from a traversal thus prolongs immediately, i.e. in the same traversal, to the worker. Data is sent from the worker back to the master when the worker terminates. Fine-to-coarse data propagates immediately in the same traversal.

Horizontal data exchange is asynchronously realized by non-blocking MPI. Vertex copies and their data are sent out from one rank to all other ranks holding a replica once they have been processed by the traversal. It is received prior to the first re-read of a vertex in the subsequent traversal. We therefore throttle the refinement with a marker-refine scheme: Ranks may trigger a refinement or coarsening, respectively, in one iteration. It however is not realised along a parallel boundary before the subsequent traversal where all ranks holding a replica of a vertex have received the grid modification request. Both data exchange patterns apply to stacks and heaps.

The usage of the Peano SFC simplifies and speeds up the realization of the horizontal data exchange. Let v_a and v_b be two vertices held both on rank R_1 and R_2 . We align the traversal orders on both R_1 and R_2 such that v_a is used for the last time before v_b on both ranks. Each rank thus can send out v_a immediately to the other rank once v_a has been used for the last time. The exchange of v_a is automatically hidden behind the remainder of the traversal (finishing work on v_b , e.g.). In practice, multiple vertex sends are grouped into one chunk of data to reduce MPI overhead.

We reiterate that Peano’s projection onto the surface of a partition yields a Peano curve of a reduced dimensionality [62] and thus totally orders all vertices/faces on any subpartition. As a result, the data exchange between any two ranks can be modelled by one channel/stream and no reordering of any incoming data is required as long as we invert the traversal on all ranks after each grid sweep [16]. v_a is sent out before v_b . The send of v_a is hidden behind the treatment of v_b . v_b is read in the subsequent iteration from the remote rank before v_a .

Design decision 12. Peano exploits the fact that the Peano SFC projected onto a partition boundary yields a $d - 1$ -dimensional Peano SFC [62]. This makes all data exchange streams without any reordering. To stick to this paradigm, we disable all DFS-BFS transformations along MPI boundaries.

To realise this disabeling, we set the markers in (2) for all cells along an MPI boundary to \perp . A hybrid MPI+X code runs MPI globally, the grid skeleton per rank remains single core, and it triggers shared memory parallelization only on interior enclaves [52].

7.4 Parallel programming interface

Peano’s non-overlapping strategy with its logic tree topology is mirrored by additional events (Table 5). MPI Peano applications are strict extensions of a serial code base. No behaviour of serial events is altered. The main control loop is ran only on rank 0 (global master), and any choice of a particular mapping to be ran is automatically broadcasted to all working ranks. Upon an `iterate`, the global master’s traversal automaton starts to run through its tree and recursively triggers traversals on all other ranks’ spacetrees. Per rank the same event set is invoked.

Dynamic load balancing is hidden from the events. A distinct set of event-like plugin points does exist. Due to them, we may realise various load decomposition schemes controlling which subtrees are deployed to (which) new ranks or which master-worker decompositions shall be removed due to a tree merger. As out-of-the-box, proof-of-concept solution, Peano comes along with a greedy spacetree decomposition.

7.5 Communication reduction and elimination

One showstopper in obtaining parallel scalability is any algorithmic synchronization (lock stepping). Synchronization in Peano materialises notably as vertical data exchange. To streamline the master-worker communication, we allow the global master to run a fixed number of grid traversals. All MPI ranks are then informed beforehand about this fixed number of traversals. At the same time, users may specify that local automata do not require information from coarser levels in these sweeps. Each rank thus runs a fixed number of iterations and couples to its multiscale neighbour, but the ranks are not globally synchronized with each other. We call one set of grid sweeps a batch.

The other way round, users can specify whether and which data is to be sent from workers to masters upon completion. This mechanism unfolds its full potential once we clarify that the wake-up call from a master decides whether vertical data transfer is required on a per rank per grid sweep base. Every time a worker traversal is started, the aligned event `prepareSendToWorker` on the master returns a flag, Peano memorises this flag and, depending on it, skips the reduction from this worker.

Besides vertical information, the code also offers routines to switch off horizontal data exchange via the stacks, users can minimize the horizontal data transfer through the heaps by sending out only those vertices/attributes that have changed, and we support algorithms that send out heap data in one iteration but receive it n iterations later. This allows us to interweave grid traversals into a communication-demanding scheme: data sent out in one iteration is allowed to run through the network while other grid traversals are executed.

Design decision 13. Peano’s default is a non-replicating scheme where all traversal automata are synchronized vertically both top-down and bottom-up. Yet, we allow the user codes to skip either synchronization. This decision can be made autonomously by each master per worker per grid traversal.

If all master-worker data flow is masked out, Peano’s communication patterns resemble replicating schemes. All tree automata start to traverse, though with level shifts, at the same time. If all worker-master data flow is eliminated, too, and global synchronisation is realised by the user within the events manually through MPI calls, the overall communication scheme is exactly the same as in a replicating strategy.

7.6 Limitations of the approach

It remains open whether replicating or non-replicating spacetree decomposition are superior. Non-replicating schemes tend to synchronise tighter, replicating schemes come at the cost of more data to be held consistent. They nevertheless seem to be more straightforward to program as synchronisation does not block other ranks to continue their traversal. It thus might be reasonable, in the future, to offer both alternatives. Overlapping schemes fit into the presented mindset and have successfully been applied to spacetrees and SFCs. It however is unclear, to the best of the author’s knowledge, how the overlaps interplay with the data flows of a scheme that remains non-replicating wherever possible.

It is in this context important to observe that our distinction of bottom-up and top-down decomposition starts to blur depending on the usage: If solely data on the finest grid is held, DFS in its unmodified form does not serialise the distributed tree traversal. While we can filter out grid events on coarser levels on a per-rank basis, i.e. for the non-distributed algorithm part, our code base also allows us to switch off reduction. This can be seen as parallel counterpart to the filtering. It makes the traversal pick up characteristics of leaf-only codes as detailed in the experiments. We finally remark that bottlenecks in reductions often are mitigated by the introduction of a tree structure and replication of coarse grid nodes.

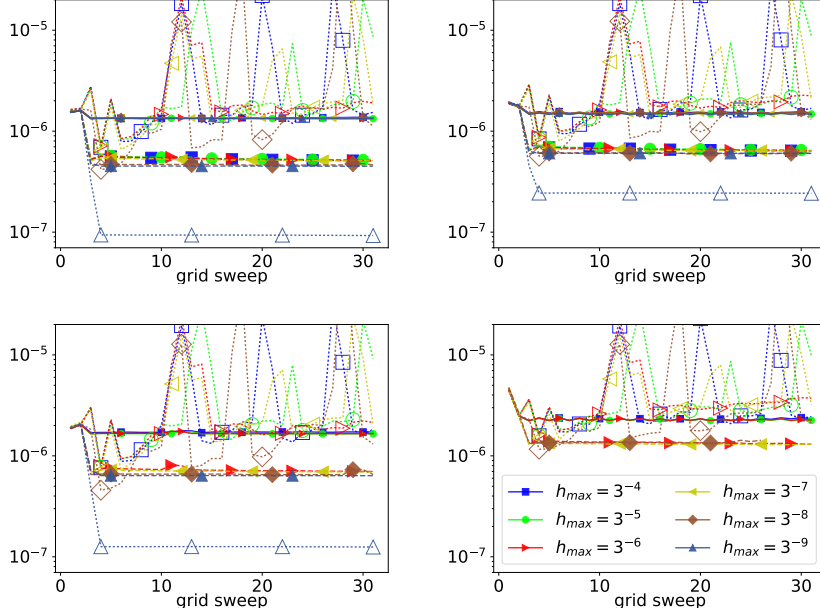


Figure 7: Cost (real time) per grid sweep per vertex on a Hamilton node. $d = 2$ with $h_{min} = 3^{-9}$ where the “stimulus” circle moves 0.01π per grid sweep. We compare two doubles per vertex held on stacks (left, top) to two doubles per vertex held on a heap (right, top) to 28 doubles administered through stacks (left, bottom) to 768 doubles per vertex held on a heap (right, bottom). The $h_{max} = h_{min}$ setup is too memory-demanding for 768 doubles per grid entity.

8 Experiments

We close our discussion with benchmarks to uncover some of the performance characteristics tied to the grid management, traversal and programming paradigm. Our tests restrict to properties studied separately from each other. Real-world examples bringing together space-trees with applications and thus also interweaving the individual properties are beyond scope. Examples for such configurations are discussed in the appendix. Despite the lack of application context, we report runtime cost per grid entity—a quantity which has to change if an application plugs into Peano.

All experiments are conducted with various doubles held per vertex plus various FLOPs ran per double on Durham’s cluster Hamilton with Intel Xeon E5-2650 v2 (Ivy Bridge) nodes with 16 cores per node at 2.6 GHz or on SuperMUC hosting Sandy Bridge-EP Xeon E5-2680 processors at 2.7 GHz. Furthermore, we run some experiments on an Intel Knights Landing chip (Xeon Phi 7250) at 1.40GHz. All shared memory tests rely on Intel’s Threading Building Blocks (TBB).

Throughout the experiments, we manually prescribe the adaptivity: We first fix a minimum and a maximum grid resolution ($h_{min} \leq h_{max}$). If they are equal, we study a regular grid. Otherwise, we refine around a circle within the domain to the finest spacetree level meeting h_{min} and coarse outside of this circle up to the coarsest mesh level meeting h_{max} . No balancing [33, 48, 53] is imposed. For non-stationary tests, the “refinement” circle follows an ellipsoidal trajectory.

8.1 Characteristics of the storage schemes

We start our experiments with single core measurements where we eliminate all floating point operations from the code. Per vertex, we hold only two doubles. Runs on the Ivy Bridge (Figure 7) compare a plain realization to a realization exploiting the grid regularity through

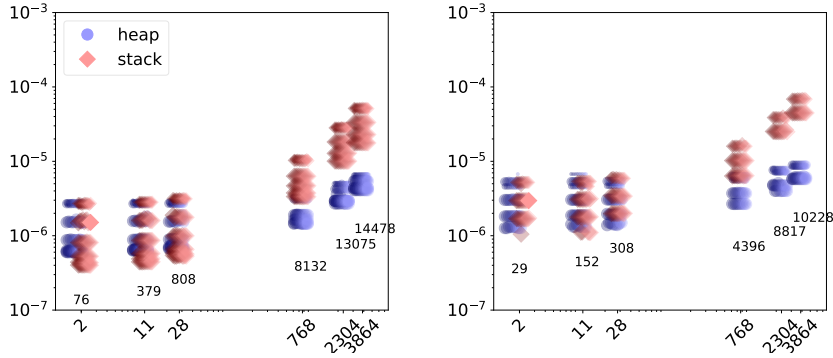


Figure 8: We compare, from left to right, increasing setups of number of doubles per grid entity (vertex). The y-axis gives cost per vertex (real time per vertex per sweep) on a SuperMUC core for stack-based (diamond) and heap-based (circle) data management. $d = 2$ (left) results face $d = 3$ data (right). The brighter the colour and the more we shift the symbol to the right, the more flops per grid entity: we run from 1 up to 1024 flops per vertex. The bigger the symbol the more vertices are generated by the dynamic adaptivity criterion. Stack and heap symbols are slightly displaced to help us to distinguish them if they clutter. We annotate each code configuration with its best-case memory throughput as MByte/s.

an on-the-fly switch into BFS as well as a realization storing regular subtrees separately. The latter two complete a kick-off phase spanning three iterations where first the initial grid is constructed and then (2) is determined. Only the third sweep benefits from $f \geq 0$. Runtime peaks are caused by memory allocations for the regular subtrees.

Observation 6. In the plain algorithm formulation, the cost per vertex is almost agnostic of refinement pattern.

Our deterministic grid traversal of a linearized spacetime pipes two data streams—one for the cells, one for the vertices—through the system (Figure 3.2). Temporary, intermediate storage resides in the caches. Refinement or coarsening triggers stream insertions or the removal of elements from the output stream. This yields, despite the dynamic adaptivity, data accesses with high spatial and temporal locality [38] and, hence, high cache hit rates [15, 42, 59, 62].

An evaluation of (2) and an on-the-fly switch to BFS for regular subtrees speeds these traversals up by around a factor of two and remains independent of the adaptivity pattern. Refinement and erase are localised per grid sweep. Remaining unaltered grid regions thus have to cause the performance improvement. For them, there is an overhead through the traversal reordering that is compensated by the simplified event invocation and the elimination of case distinctions.

Observation 7. On-the-fly tracking of regular subtrees pays off. Replacing regular grid regions within the tree pays off if the grid does not change often, if the regular subtrees held separately are sufficiently large, and few doubles are held per grid vertex.

Cutting out regular subgrids from the overall grid is delicate as we have to keep the redundant vertices between the grid regions consistent. This administrative overhead is only amortised if the persistent subregions are very large ($h = 3^{-9}$ here) or the grid is stationary (not shown). Large is to be read as ratio of number of grid entities per subtree to number of unknowns per vertex.

We reiterate that the selling point of the regular subtree identification is not primarily serial speed but an increase of the concurrency level. As such, our measurements establish a performance baseline and show how this baseline correlates to unaltered grid traversals. Recursion unrolling with properly configured thresholds from which on it pays off to replace subtrees is used from hereon.

We continue with single core measurements (Figure 8) that compare stack- to heap-based

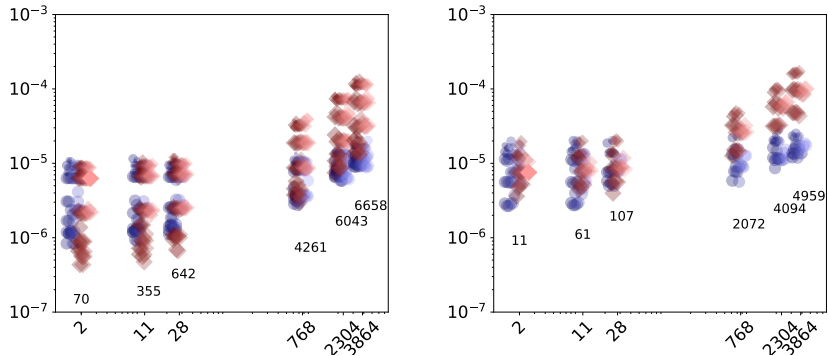


Figure 9: Experiments from Figure 8 reran on the Intel KNL architecture.

unknown storage. For $d = 2$, they reveal that an embedding of application-specific data into the spacetime stream is advantageous if and only if the number of doubles per vertex is small. As soon as we store more than a few doubles, it is advantageous to separate the spacetime stream from the actual user data. For large data cardinalities, we otherwise quickly loose up to an order of magnitude of performance. The $d = 3$ grid administration is by at most a factor of two more expensive than its 2d counterpart, though the difference vanishes once the number of unknowns per grid entity grows large. The actual arithmetic cost per grid entity on one core does not make a difference here. For the three setups with a small memory footprint per grid entity our approach is spacetime administration-bound as the throughput is flat. From 768 doubles per vertex on, the runtime increases with increasing data cardinality. The code’s administration overhead team up with data squeezing through the memory interconnect.

All statements transfer qualitatively to the manycore (Figure 9) though the results become more fuzzy. Notably, a heap-based unknown storage seems to pay off for $d = 3$ immediately. On the KNL, Stream TRIAD yields around 11,366 MB/s. For a single core the spacetime code exploits only half of the best-case single core throughput. This is the spacetime/adaptivity administration overhead. The difference in throughputs on the two architectures directly correlates with the difference in clock rates.

Observation 8. For very small data cardinalities per grid entity and rapidly changing grids, it pays off to merge the compute data into the grid data. Otherwise, it is better to separate the two containers. For a few hundreds of unknowns per grid entity, the multiscale spacetime administration cost dominate the runtime.

Our observations suggest that it is, in practice, unavoidable to use some kind of patches or high order methods with lots of unknowns per grid cell if high FLOP rates are to be obtained. With the full multiscale tree formalism, we need a significant workload to mitigate the spacetime administration overhead.

8.2 Concurrency impact of the DFS-BFS transformation

We continue with multicore experiments handling solely the finest grid level—we label those with `finegrid`—or triggering operations on all grid levels (label `multiscale`). The operations mitigate stencil (matrix-free operator) evaluations. The latter avoid race conditions between multiscale vertex accesses through proper mesh colouring with 7^d colours, while the finegrid variant succeeds with four colours in total. Again, we run the setups for various combinations of maximum and minimum mesh sizes. All experiments not employing regular grids work with dynamic adaptivity changing each grid sweep.

Various shared memory parallelization features of Peano’s traversal automaton can be switched on or off by the user code, and its traversal automaton using static problem partitioning for all parallel loops can also be fed with situation-specific grain sizes. We thus face a large range of parameter choices: which features are to be switched on and off and which

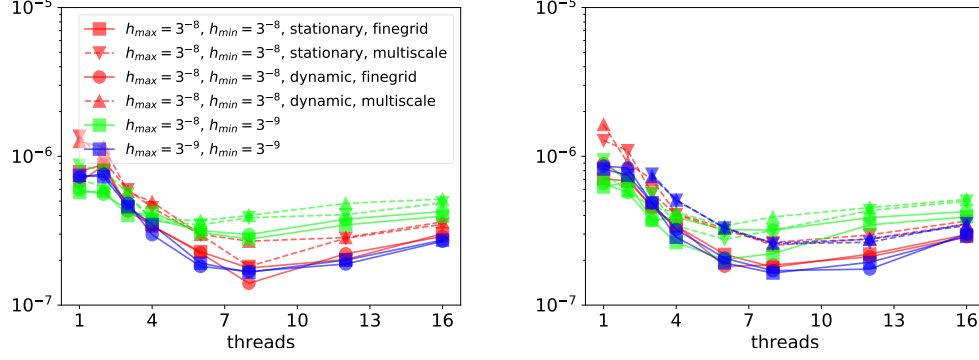


Figure 10: Two scaling curves of the DFS/BFS on Hamilton for $d = 2$ setups. Runtime per vertex per sweep. Two doubles are held per vertex. We either run 28 (left) or 256 (right) floating point operations per double per vertex.

grain sizes are to be chosen? For the present manuscript, we use Peano’s hardcoded default values.

Its outcome can qualitatively be summarized as follows: Decomposing the data load and store process along the surface of regular subtrees into tasks is robustly superior to a sequential load and store. Once we load data for $f \geq 1$, we may furthermore hide the handling of coarse levels behind the load and stores of finer levels. Significant scalability however only is predicted for the colouring of the BFS traversal phases.

The parallel efficiency obtained is limited as soon as we run into dynamically adaptive grids (Figure 10). Only if large regular sub-grids ($h = 3^{-8}$ or $h = 3^{-9}$ relative to the unit length) are encountered, we observe scaling. Variants with only fine grid manipulations scale better if the work per vertex is sufficiently high—an obvious property given the weaker concurrency constraints. Furthermore, we observe scaling for adaptive subpatterns if and only if the adaptivity pattern remains stationary. Finally, we observe that a proper grain size should scale with the problem size: If the grain size is too small relative to the problem size, our academic decomposition into tiny tasks yields a too high task administration overhead. Peano offers a plug-in point to inject proper problem size-dependent into any application. If a manual identification is too cumbersome, its toolbox collection provides a generic machine learning algorithm to derive proper grain size choices on-the-fly [19].

Strong dynamic adaptivity makes our DFS/BFS-based parallelization deteriorate from a parallelization strategy into a minor speed improvement. This teaches five lessons: First, we have to employ classic domain decomposition working with separated trees to obtain good scalability in our AMR context. This allows threads to work on separate memory regions and can be done either via MPI as studied next or with low-overhead shared memory (cmp. [49, 50], e.g.). Data decomposition has to be applied on-node, too. Second, scaling a Peano code is simplified if the basic operations per grid entity themselves exploit multiple cores (cmp. to the concepts of inter-patch and intra-patch concurrency in (author?) [60]). A pure grid-based parallelization easily falls short of exploiting all cores—if there are many cores. Third, it makes sense to (artificially) increase the grid regularity. The loss in efficiency measured by work per accuracy can be compensated by an increased scalability. Fourth, it is reasonable to evaluate where tasks can decouple from the grid traversal: the traversal automaton then identifies when a task is due, spawns the task in the background [21], but continues to traverse while the task completes. Finally, it makes sense in a multicore environment to fix the grid over multiple grid sweeps. In this case, we can eliminate all checks w.r.t. (2) and the coinciding thread synchronisation; both ideas are not applied here.

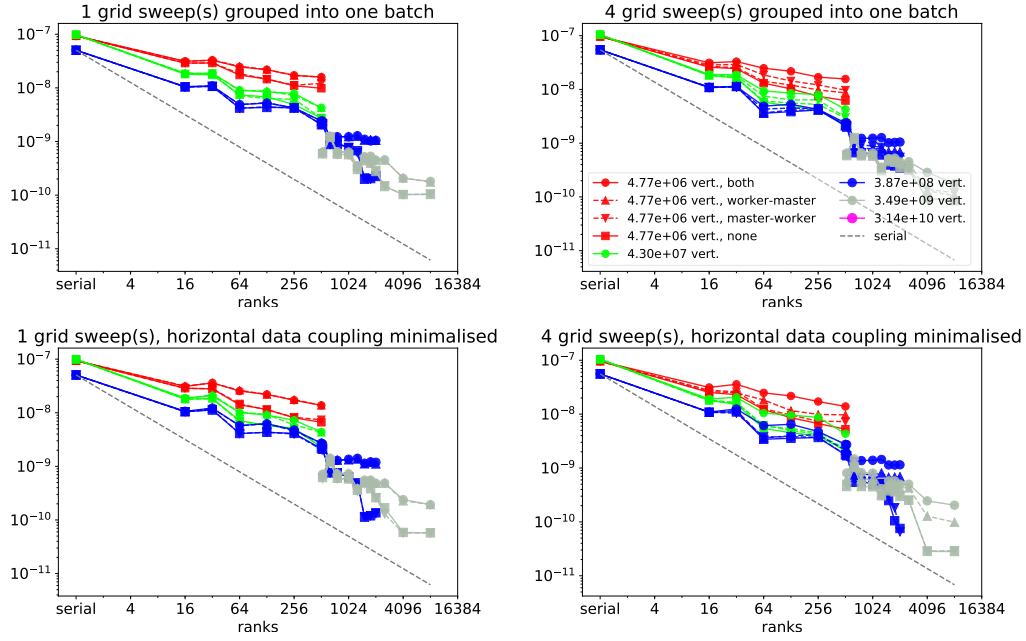


Figure 12: $d = 2$ scalability as runtime per sweep per vertex on SuperMUC. Eight doubles are assigned to each vertex. In the top row, each and every vertex along the domain boundary is exchanged with all neighbouring partitions. In the middle and lower row, vertices are only exchanged when they change their state. We either switch on vertical communication both ways, send only data from the masters to the workers, the other way round, or eliminate all vertical data exchange per batch completely, i.e. exchange vertical data only at the end of the batch. No arithmetic work is done.

Table 6: Some speedups for various (averaged) vertex counts in Ω_h where we use the Peano SFC to derive proper domain decompositions and deploy six ranks per 24 core compute node. The speedups are normalised to the smallest problem setup. We present data for 2 (top) and 768 (bottom) doubles per vertex.

nodes/ ranks	$d = 2$				$d = 3$			
	$5.90 \cdot 10^4$	$5.31 \cdot 10^5$	$4.78 \cdot 10^6$	$4.30 \cdot 10^7$	$5.31 \cdot 10^5$	$1.43 \cdot 10^7$	$3.87 \cdot 10^8$	$1.05 \cdot 10^{10}$
1/6	2.89	4.39			2.13	3.99		
2/12	10.1	13.4			3.04	4.79		
4/24	10.4	12.4	20.9		3.07	13.7	17.0	
8/48	10.7	21.2	32.2		3.05	9.35	23.6	
12/72	11.3	24.2	34.4		3.05	9.28	24.5	
16/96		29.6	85.2			9.26	24.6	79.7
1/6	1.59	2.48	3.52		0.84	2.13	4.05	
2/12	1.35	8.74	12.7		0.78	3.03	4.84	
4/24	2.72	8.39	11.0	19.4	0.77	3.05	14.0	17.2
8/48	3.00	8.85	17.9	28.1		3.04	9.38	23.9
12/72		8.97	19.5	30.7				
16/96			40.0	86.9				

within a batch. If we compare an elimination of worker-master to worker-master information exchange, a skip of the reductions contributes more to good scalability. This diversification w.r.t. vertical data exchange becomes observable when the graph enters the strong scaling stagnation regime. For several setups it can invert the classic strong scaling behaviour, i.e. the expectation that a simulation scales the better the more detailed the grid that is used is. This behaviour is reasonable once we emphasise that finer grids couple individual ranks stronger through horizontal data exchange than shallow grids.

Observation 10. The elimination of vertical data exchange in combination with batching allows us to decouple ranks that do not exchange a significant amount of data through the domain boundaries.

The advantageous behaviour with the data exchange skips is contrasted by steps in the scalability graphs: as we cut through the spacetree in a top-down fashion, optimal scalability is obtained if and only if the number of ranks matches the grid structure. For a $2d$ regular grid, a rank count of nine for example allows us to split up the grid properly. If only two ranks are available, a proper splitting exhibits an ill-balancing of 4:5. The master-worker topology however permits only ratios of 1:8. The effect becomes stronger for $d = 3$ (not shown) and explains the plateau at 4.096 ranks. The step effect becomes less dominant once (varying) arithmetic work is done per grid entity.

Observation 11. The master-worker MPI topology restricts the admissible fine grid partitions, i.e. most reasonable fine grid splittings cannot be mapped onto a master-worker topology. While the non-replicating scheme minimizes the data and work done per rank, it struggles to compete with replicating schemes.

There are two straightforward solutions to this challenge. We either can combine a non-replicating scheme on coarser resolutions with a replicating domain decomposition for finer scales. This is subject of future work. Or we can deploy multiple MPI ranks per compute node, derive a proper domain splitting—in Peano’s case using the Peano SFC is a natural candidate—and ensure that workers responsible for subdomains neighbouring along the SFC are deployed to the same rank. This technique smoothes out the scalability to some degree (Table 6) once the ratio data per vertex relative to the mesh size becomes reasonably small. It seems to be particularly promising for applications that cannot exploit all cores through shared memory parallelisation. It seems not to be promising for $d = 3$ setups with massive data per vertex and, thus, massive communication demands. We however emphasise that our results in Table 6 are biased as we strip the code off any computation.

Cutting a tree into distributed memory pieces has the advantage that it suits both distributed and shared memory machines. We close our distributed tree discussion by running

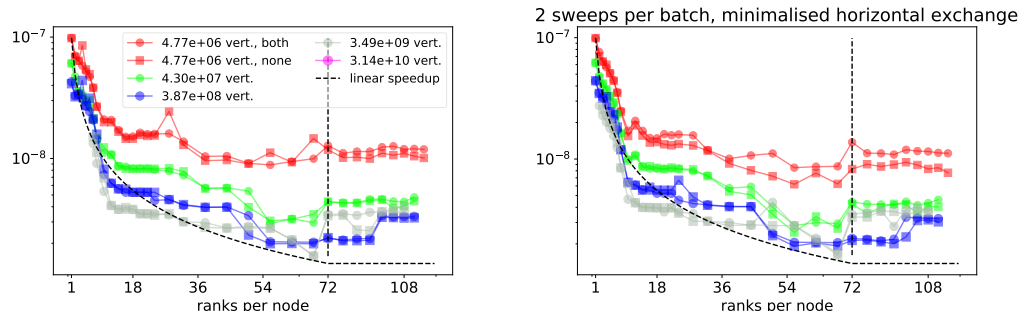


Figure 13: Cost as time per sweep per vertex for $d = 2$ on one KNL node with 72 cores. The spacetree is decomposed into subtrees and distributed via MPI. No BFS parallelisation is enabled.

the tree decomposition on a manycore architecture as alternative to our DFS/BFS transformation. The latter is orthogonal, i.e., it can be combined with the decomposition. Our results (Figure 13) suggest that such an on-node strategy can yield another speedup of close to a factor of almost 20 with high efficiency. Going beyond a factor of 20 or overloading do not pay off. We notably should refrain from booking all cores for the computation. Vertical data exchange or its skipping, respectively, do not play a major role for larger trees. They unleash their power in-between the nodes.

Observation 12. A mixture of tree decomposition with on-the-fly BFS/DFS transformations is a promising strategy to exploit manycore architectures.

9 Conclusion and outlook

The present paper introduces a software framework for dynamically adaptive multiscale grids that fuses data management and data traversal as well as, if not explicitly outsourced to a heap, application data storage. The underlying programming model is formalized with two automata yielding an event-based algorithm development approach. Besides the fact that the software delivers a merger of multiple state-of-the-art features such as support for arbitrary dimensions, multiscale data representation and low memory footprint capabilities, it is reasonably simple to handle due to its restrictive, minimalistic programming model. This makes the software well-suited for fast prototyping as well as bigger codes with a clear separation of concerns as long as they accept the restrictive academic programming paradigm which might imply that not each legacy code can directly use the AMR features.

The manuscript characterizes, classifies and motivates several design decisions made while the framework was written. It also explicitly highlights shortcomings and open questions notably in comparison with other approaches found in literature. The references to alternative pathways towards realisation are backed up with some experiments that highlight that the software is capable to code sophisticated applications running in parallel. Yet, the discussion and the results also highlight that other spacetree code developers might favour other realisation variants that are superior for particular challenges.

There are two natural directions of future work. Both start from the observation that the present discussion is very academic and computer science-centric. It lacks challenges from real-world computational simulation codes that either rely on the present software stack, some of its components or discussed paradigms. On the one hand, it is important to track their code maturity, maintainability and clarity once we “scale” up the code w.r.t. simulation detail complexity. This will allow us to assess and understand the limitations and drawbacks imposed by the present programming model from a usability point of view. It also might help to identify ways to make the software easier accessible without giving up its clarity and clear separation of concerns.

On the other hand, it is important to track the computational and algorithmical efficiency

of application codes. Our case studies reveal that there is scalability potential arising from the present code base. Yet, this scalability, though we restrict to worst-case studies that will not be found this way in applications, is far from optimal and will drive future developments. We see notably potential in mergers of replicating and non-replicating tree decomposition schemes and in the combination of our grid-based task model with tasking approaches where tasks are decoupled from the grid entities and can run in parallel to the grid traversal.

Acknowledgements

The author appreciates support received from the European Unions Horizon 2020 research and innovation programme under grant agreement No 671698 (ExaHyPE). This work made use of the facilities of the Hamilton HPC Service of Durham University. The author furthermore gratefully acknowledges the Gauss Centre for Supercomputing e.V. (www.gauss-centre.eu) for funding this project by providing computing time on the GCS Supercomputer SuperMUC at Leibniz Supercomputing Centre (www.lrz.de). Finally, this manuscript particularly has been benefitting from the support of the RSC Group who granted us early access to their KNL machines. All underlying software is open source [61].

A Software base

Peano is freely available from [61]. We offer both tarballs and repository access through Subversion. Support is provided through a maillist. An extensive guidebook discusses how to implement solvers in Peano. It also comprises case studies.

The code baseline offers support for adaptive Cartesian grids [3, 9, 18, 24, 30, 34, 35, 37, 40, 47, 48, 51, 53, 55, 56] as discussed in the manuscript. It thus follows an academic approach to AMR programming and lacks the flexibility and generality of software alike (**author?**) [1, 8, 9, 10, 11, 20].

Extensions of the sole grid and its traversal are available via a template mechanism and small routine collections (toolkits) that inject plotting facilities for Paraview/VisIt, realize shared memory autotuning [19] or add dynamic load balancing based upon graph partitioning or the underlying Peano space-filling curve. Further examples for toolkits are routine collections for matrix-free multigrid [46, 58], Particle-in-Cell features [63] similar to [37] or patch-based PDE solvers [60]. The latter allows users to compose the AMR grid as assembly of regular patches and makes the software resemble block-structured AMR alike (**author?**) [1, 20], e.g.

While the domain decomposition relies on MPI using [13, 17] to generate user-defined MPI data types, the software currently offers bindings to OpenMP 4 and TBB for task-based parallelisation. These bindings are hidden through a software layer. With task approaches having successfully been used in various spacetime and non-spacetime codes such as [20, 43, 57], the bindings could be replaced by a more sophisticated task subsystems.

B Examples on statements from paper

This section comprises a few examples illustrating statements from the manuscript. To compact the presentation, examples stick to bipartitioning ($k = 2$) and two dimensions ($d = 2$) if not stated otherwise. Most examples illustrate concepts with the help of Figure 14. The examples clarify statements from the text but also clarify that most manuscript concepts are not tied to tripartitioning which is used in Peano’s code base.

Section 2 picks up classic tree enumerations applied here to adaptive Cartesian grids. We illustrate some classic textbook orderings with the help of the example tree.

Example 1. For the spacetime in Figure 14, we write down following orderings:

- Depth-first, Morton/z-curve ordering:
A, B, I, G, Q, R, O, P, F, H, D, J, S, T, U, V, M, Y, Z, W, X, L, N, C, E

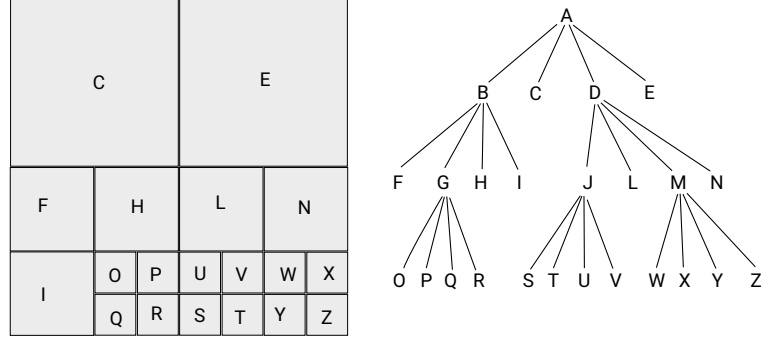


Figure 14: Illustration of an adaptive Cartesian spacetree grid for $d = 2, k = 2$ (left) with its tree (right). The labels do not follow any particular SFC but are arbitrarily chosen along a DFS.

- Breadth-first, Morton/z-curve ordering:
A, B, D, C, E, I, G, F, H, J, M, L, N, Q, R, O, P, S, T, U, V, Y, Z, W, X
- Depth-first, Hilbert ordering:
A, B, I, G, Q, R, P, O, H, F, C, E, D, N, L, J, V, U, S, T, M, Y, W, X, Z
- Breadth-first, Hilbert ordering:
A, B, C, E, D, I, G, H, F, N, L, J, M, Q, R, P, O, V, U, S, T, Y, W, X, Z

The core spacetree enumeration in Peano is never computed explicitly. Instead, all numbering is given implicitly by the ordering within the streams. We nevertheless quickly reiterate explicit tree orderings, as they help to digest the linearization discussions and can be of help to study heap storage techniques where the spatial plus level position of a grid entity acts as preimage to the hashing function. A (historical) overview of SFC numberings, related publications and their relation to text replacement systems can be found in [4], e.g.

Example 2. For the spacetree in Figure 14 and depth-first Morton order, we study the cell P . In a binary basis, it is encoded by 00|01|11 (use the first cell (00) on level 1, then descend into the second (01) cell along the SFC on level 2; finally pick the third cell on level 3 within the cell chosen before) and each digit d -tuple describes a subcell. We can derive a child's position within its parent from the tuple's d entries. Furthermore, the code allows us both to determine the cell's spatial position and size within the grid as well as neighbour relations, i.e. to look up a neighbour on any level, we can manipulate the code and directly check whether a cell with such a code exists. For $k = 3$, we have to choose a ternary base.

Section 3 and other statements in the manuscript clarify that Peano supports unbalanced grids (compare the 2:1-balanced grid in Figure 14 to the unbalanced grid in Figure B). Proper grid balancing might simplify and speed up any explicit assembly for example as it constrains the matrix bandwidth. Another application domain of interest are explicit hyperbolic DG solvers where grid balancing reduces discretisation errors. Both benefit from 2:1 balancing. Yet, there is no need to enforce it by the grid code always. Users may switch on balancing which identifies on-the-fly whether any resolution transition between two neighbouring cells exceeds one level of refinement and, if this is the case, refines the coarser cell in the subsequent grid sweep. Such a primitive approach causes a delayed rippling, i.e. grid balancing is not immediately enforced but propagates successively through the grid. If perfect balancing is mandatory, any grid modification has to be followed by a while loop converging the grid into a balanced variant. More sophisticated algorithms are known [33, 53] yet have not been implemented yet. Peano offers a toolbox to inject the non-sophisticated balancing into the grid.

Adaptive Cartesian grids yield hanging nodes such as the vertex adjacent to I, O, Q. As Peano makes a vertex unique through its level plus its position, also the vertex adjacent to I, O, F, H is hanging, while its parent vertex adjacent to F, G, H, I is not hanging.

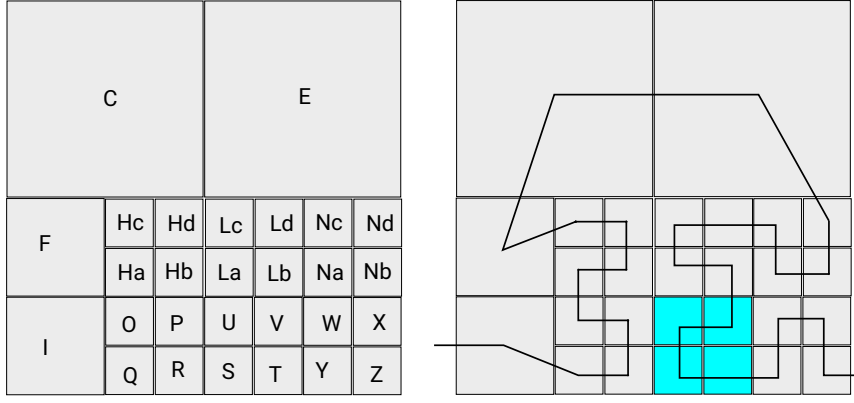


Figure 15: Left: Illustration of a non-balanced tree where cells (Lc and E, e.g.) are adjacent that differ by more than one level. Right: Traversal of the grid along the Hilbert SFC.

Peano’s event signature from Table 2 ensures that a pair of `createHangingVertex` and `destroyHangingVertex` events is triggered as least once per traversal per hanging vertex. However, the framework is free to trigger create-destroy pairs more often, i.e. to remove hanging vertices temporarily throughout the grid sweep.

Example 3. In the following example, the tuple subscript of indices identifies all adjacent cells of a vertex. We show exemplarily how the lifecycle of hanging vertices integrates into (1). For the grid from Figure B we obtain

```

touchVertexFirstTime( $v_{I,G,F,H}$ )  $\sqsubseteq$  enterCell( $I$ )
enterCell( $G$ )  $\sqsubseteq$  enterCell( $O$ )
touchVertexFirstTime( $v_{I,G,F,H}$ )  $\sqsubseteq$  createHangingVertex( $v_{I,O,F,H}$ )
touchVertexFirstTime( $v_{I,G,F,H}$ )  $\sqsubseteq$  createHangingVertex( $v_{I,Q,O}$ )
createHangingVertex( $v_{I,Q,O}$ )  $\sqsubseteq$  enterCell( $O$ )
leaveCell( $O$ )  $\sqsubseteq$  destroyHangingVertex( $v_{I,Q,O}$ )
destroyHangingVertex( $v_{I,Q,O}$ )  $\sqsubseteq$  touchVertexLastTime( $v_{I,G,F,H}$ )

```

The last constraint in the example is not completely describing the grid behaviour. As long as no other constraint is harmed, the traversal automaton may destroy hanging nodes (and invoke the corresponding destruction) and then on-the-fly recreate them invoking the creational event. Hanging nodes are never persistent. Yet, a user always can use a hanging node’s position plus level to hold hanging vertex data on the heap.

The on-the-fly computation of (2) in Section 5 is one of the pillars of Peano’s traversal optimisation, as it facilitates recursion unrolling. Recursion unrolling in turn yields cascades of regular Cartesian grids that on the one hand enable us to traverse these sub-data structures along BFS or to outsource the regular subtrees in the memory.

Example 4. Let S, T, U, V from Figure 14 each be refined once more. After one traversal, $f(J) = 2$ following (2). When the traversal automaton runs into J , i.e. loads it from the input stream, it can load the following $(2^1)^d + (2^2)^d$ cells en block from this stream. A similar reasoning holds for the accompanying vertices. The automaton then invokes `touchVertexFirstTime` for all vertices adjacent to S, T, U, V that have not been touched before, it then invokes `enterCell` for S, T, U, V , it then invokes `touchVertexFirstTime` for all vertices adjacent to children of S, T, U, V , and so forth. Finally, the whole subtree is piped into the output streams.

Studying Figure B, we can illustrate all statements on the boundary exchange between regular subtrees and the spacetree. We assume that the coloured region of cells S, T, U, V plus their

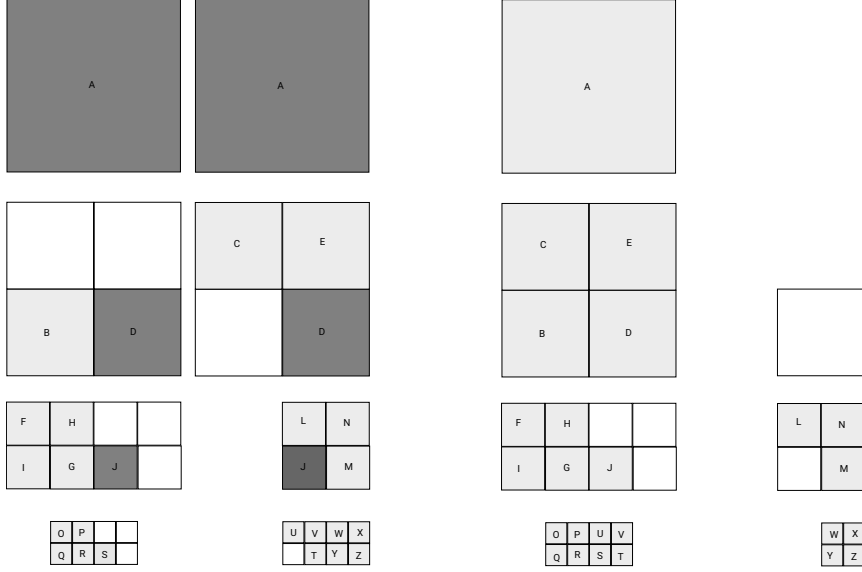


Figure 16: Left: Bottom-up splitting of tree from Figure 14—a variant Peano does not support at the moment. Dark cells here are cells held redundantly by both ranks. Their data has to be kept consistent. White cells are cells not handled by the local rank. Their sole purpose is to make the local data structure a proper spacetree. Right: Top-down splitting as used by Peano with the left rank being a master of the right rank. No data is held redundantly.

parent J are identified as regular subgrid and held separate from the remaining subtree. The remaining subtree is an adaptive Cartesian spacetree grid with holes.

Example 5. If we have an SFC traversal of the grid as illustrated in B and outsource the marked grid region as regular subtree, the following properties hold:

- Peano holds the vertex $v_{R,S,P,U}$ redundant, i.e. within the holed spacetree, i.e. the skeleton grid remaining after we have cut out regular subtrees, and as part of the outsourced regular subtree.
- Within the subtree, Peano reorders the grid traversal BFS lexicographically (J, S, T, U, V) or subject to given constraints/colouring schemes.
- The consistency updates between regular subgrid and holed spacetree exploit the fact that the SFC orders all vertices along the interface. Let the holed spacetree enumerate the vertices with $v_{R,S,P,U} \subseteq v_{P,U,Hb,La}$ and temporarily dump the vertices along this order. Once the traversal automaton enters the regular subtree, it is aware of the SFC and can read in/copy the subregion’s surface vertices along this order.

The exchange between regular subtrees and the holed spacetree grid here is illustrated for the Hilbert SFC. For $d = 2$, such an illustration is straightforward. The extension to $d = 3$ is cumbersome for Hilbert. Peano however uses the Peano SFC which has the advantageous property that the SFC’s projection onto the surface of the regular subgrid is a Peano SFC of dimension $d - 1$ [62]: The vertex enumeration along the subdomain’s boundary is continuous and the enumeration itself “meanders” over the surface again, while two adjacent ranks exchange all data in the same order, i.e. no reordering is required.

We continue with statements on Section 7, notably with references to other software solutions relying on a bottom-up SFC partitioning [3, 18, 27–30, 43, 48, 51, 53]. For our examples, let $J, L, D \in \mathcal{T}$ with $J, L \subseteq_{\text{child of}} D$ and L handled by a worker of the rank responsible for D and J . Let D descend into L and trigger the traversal of the subtree rooted by L . If the worker-master consistency check from (1) integrates into the recursion unrolling, the rank may not continue with J before the traversal of the remote automaton handling L terminates (Figure 16).

Example 6. The Morton order from Figure 14

A, B, I, G, Q, R, O, P, F, H, D, J, S, T, U, V, M, Y, Z, W, X, L, N, C, E
is rewritten level-wisely depth-first into
A, B, D, C, E, I, G, F, H, Q, R, O, P, J, M, L, N, S, T, U, V, Y, Z, W, X.

Example 7. We study Morton orders from Figure 14 on two processes that split up after cell S. The tree is processed by two ranks with a replicating DFS scheme as

Rank R1: A, B, I, G, Q, R, O, P, F, H, D, J, S, T(e), U(e), V(e), M(e), L(e), N(e), C(e), E(e), sync(J, D, A)

Rank R2: A, B(e), D, J, S(e), T, U, V, M, Y, Z, W, X, L, N, C, E, sync(J, D, A)

cells with addendum (e) are empty, i.e. replicated to create a valid octree though they hold no data.

For a non-replicating scheme, we deploy the cells M, L and N along the SFC—they are all on one level and thus preserve trivially the logic tree topology between the ranks—and run level-wisely DFS through the tree:

Rank R1 (master): A, B, D, C, E, I, G, F, H, Q, R, O, P, J, M(e), L(e), N(e), start-R2, S, T, U, wait-for-R2

Rank R2 (worker): wait-for-R1, J(e), M, L, N, Y, Z, W, X, sync-with-R1

Example 8. The fine grid from Figure 14 has 19 fine grid cells in Ω_h . An optimal load balancing for four ranks r_0, r_1, r_2, r_3 assigns four or five cells to each rank. If we use the Hilbert ordering, a splitting could read

$$\begin{aligned} r_0 &\mapsto \{I, Q, R, P, O\} & r_1 &\mapsto \{H, F, C, E, N\} \\ r_2 &\mapsto \{L, V, U, S, T\} & r_3 &\mapsto \{Y, W, X, Z\}. \end{aligned}$$

This decomposition of the tree does not yield a master-worker topology.

An admissible decomposition would be

$$\begin{aligned} r_0 &\mapsto \{I, H, F\} \text{ plus } B & r_1 &\mapsto \{Q, R, P, O\} \text{ plus } G \\ r_2 &\mapsto \{N, L, V, U, S, T, Y, W, X, Z\} \text{ plus } D & r_3 &\mapsto \{C, E\} \text{ plus } A \end{aligned}$$

which is not well-balanced. One solution to this is to use up to four ranks per node, i.e. to subdivide the problem logically further and to construct

$$\begin{aligned} r_{0a} &\mapsto \{A, B\} & r_{1a} &\mapsto \{C\} & r_{2a} &\mapsto \{E\} & r_{3a} &\mapsto \{D\} \\ & & r_{1b} &\mapsto \{H\} & r_{1c} &\mapsto \{F\} \\ r_{2b} &\mapsto \{N\} & r_{2c} &\mapsto \{L\}. \end{aligned}$$

which yields a more advantageous partition that both fits to the master-worker paradigm on the tree, obeys a SFC-based partitioning, yields—per node—face-connected partitions, and is reasonably balanced.

C Remarks on some Peano applications

In Section 3.1, we sketch which types of applications do fit to our restrictive API. The present section substantiates these statements with examples from recent projects.

Low-order, d -linear finite element examples In [46, 58], we study variants of geometric-algebraic multigrid solvers for Helmholtz and convection-diffusion equations (Figure 2). The Helmholtz setup studies high-dimensional grids with complex-valued grid spacing, while the convection-diffusion studies derive mergers of algebraic and geometric multigrid algorithms that combine the geometric efficiency and memory modesty with the algebraic robustness. Both papers introduce single-touch algorithms and both study low order discretisations, i.e. compact 9-point stencils ($d = 2$), 27-point stencils ($d = 3$), ... They solve the PDEs

$$\begin{aligned} -\Delta u + k^2 u &= b & \text{and} \\ -\nabla(\epsilon \nabla) u + v \cdot u &= b \end{aligned} \tag{3}$$

with $u \approx \sum_i u_i \varphi_i$ through a Ritz-Galerkin formulation where φ_i is a d -linear shape functions centred around a non-hanging vertex on $\Omega_{h,\ell}$ and spanning 2^d cells.

Both papers use full approximation storage (FAS), i.e. they store a real representation of solution on each and every grid level. They work on generating systems. This renders the treatment of hanging vertices straightforward. It exploits the fact that Peano holds the individual grids $\Omega_{h,\ell}$ separately, i.e. each vertex is unique through its level plus position and multiple vertices coinciding spatially can hold different data: fine grid vertices membering Ω_h encode the solution while coarser vertices at the same position hold FAS data plus multigrid correction terms. As all stencils are compact, they decompose additively over the 2^d adjacent cells and thus can be evaluated element-wisely.

We augment each vertex by a residual holding a vertex's $r = b - Au$ contribution if A is the system matrix arising from (3). Our application automaton plugs into `touchVertexFirstTime` to set $r \leftarrow 0$. Within `enterCell`, it reads in the 2^d r, u and b values and contributes the residual contributions from the respective cells. The residual is accumulated. When the traversal automaton triggers `touchVertexLastTime`, we know that the residual for one vertex is accumulated completely, and we can trigger a smoothing step or residual restrictions. As Peano offers the opportunity to plug into the traversal automaton's steps up and down in the tree, inter-grid transfer operators can be realised "element-wisely", too.

The Helmholtz setup stores all quantities directly within the vertices, i.e. it fuses spacetree grid data and solution values. Each vertex holds one double being the weight u_i within (3) plus the discretised right-hand side. Additional temporary variables holds the residual, hierarchical residuals, error estimators, and so forth. The convection-diffusion code starts from this data representation, too. Yet, it also stores inter-grid transfer stencils and discretisation stencils, and those quantities are held on Peano's heap as they consist of at least $2 \cdot 5^d + 3^d$ doubles and we furthermore study techniques how to convert them on-the-fly into non-IEEE representations where the resulting total memory footprint is not known a priori.

Our Helmholtz studies not only study higher-dimensional grids ($d \geq 4$), they also discuss how the solution of multiple PDEs on one grid can be merged to yield higher arithmetic intensity. In this case, multiple PDEs are stored within one grid, and the arising stencils not only tackle the individual PDEs, they also couple them which yields additional flops. Our convection-diffusion studies compare the derived solvers to a setup where each vertex holds only one integer. This integer serves as local index to PETSc [6], i.e. we compare a matrix-free, monolithic solver with Peano to a solver where Peano yields solely the discretisation, the user automaton realizes the assembly, and the actual equation system is administered and solved by a black-box solver.

Higher-order DG discretisations In the ExaHyPE project [5], we study Discontinuous Galerkin (DG) discretisations of first-order hyperbolic equations

$$\frac{\partial}{\partial t} Q + \nabla \cdot F(Q) + \sum_i \mathcal{B}_i \frac{\partial Q}{\partial x_i} = S + \sum \delta \quad (4)$$

on dynamically adaptive grids. They are subject to the explicit ADER-DG timestepping scheme. Q here is defined cell-wisely as high-order ($p \in \{3, 4, \dots, 9\}$) polynomial over the cells of Ω_h .

We make each Peano cell hold a pointer to an entry in Peano's heap. Each heap entry stores, per quantity in Q , $(p+1)^d$ weights of the Gauss Legendre weights of the cell's polynomial. The spacetree acts as meta data structure. The actual compute data, i.e. Q , are held in the heap's hash map. ADER-DG is a predictor-corrector scheme: First, the automaton runs over $\Omega_{h,\ell}$ and computes a predicted solution to (4). This is done within `enterCell`. Second, we equip each vertex with 2^d pointers to the respective adjacent cells. This allows us to traverse the grid, i.e. all faces, and solve Riemann problems to the predicted solution there. The idea here is to plug into `touchVertexFirstTime` and to equip each face with one marker bit. The bit is set to zero by `touchVertexLastTime`. Once we enter `touchVertexFirstTime`, we analyse the $2 \cdot 2^{d-1}$ adjacent faces. For each face where our flagging bit is not set, we set it and evaluate the Riemann problem. Finally, we traverse the grid's cells and bring together the predicted solution with the Riemann solves. We exploit (1): it ensures that each vertex

has been “touched” prior to `enterCell`. Consequently, all adjacent faces to a cell have been processed, too. It is one insight of the underlying project that this works with single-touch semantics, i.e. one grid sweep per time step.

Hanging vertices inherit the pointers from their parent vertices when the automaton triggers `createHangingVertex`. As a result, we can also determine neighbouring cells of any hanging vertex and handle resolution transitions. ADER-DG quickly becomes unstable in the presence of shocks. For shocks, we apply a Finite Volume solver as limiter. If limiters are present, our grid carries two solvers per cell.

Patch-based finite volume solvers In [60], we study a standard Finite Volume solver for shallow water equations

$$\frac{\partial}{\partial t} \begin{pmatrix} h \\ hu \\ hv \\ b \end{pmatrix} + \frac{\partial}{\partial x} \begin{pmatrix} hu \\ hu^2 + 0.5gh^2 \\ huv \\ 0 \end{pmatrix} + \frac{\partial}{\partial y} \begin{pmatrix} hv \\ huv \\ hv^2 + 0.5gh^2 \\ 0 \end{pmatrix} + \begin{pmatrix} 0 \\ hg \cdot b_x \\ hg \cdot b_y \\ 0 \end{pmatrix} = 0. \quad (5)$$

In the simplest variant (Figure 3), we apply a simple Rusanov flux. We store three unknown quantities per cell. In an original variant they are held within the spacetime stream. Per face, we have to hold the fluxes. As Peano does not natively provide face unknown, we store the quantities from the positions $(x + h/2, y)$ and $(x, y + h/2)$ within the vertex at (x, y) . h is the cell size. We map the staggered degree of freedom layout onto vertex and cell storage locations. Within each cell, we have, through the 2^d adjacent vertices, all data available to run the Finite Volume updates.

Few codes solving equations alike (5) use strongly adaptive meshes where single cells resolve particular properties. Adaptivity criteria here typically yield areas of refinement. We therefore next embed whole $n \times n$ patches into the individual cells, equip them with a halo layer of width one, and hold both the current and the previous solution within the patch. When the automaton triggers `enterCell`, we first fill the ghost layer and then trigger the Finite Volume scheme on the patch. This block-structured AMR also yields reasonable complex compute kernels per cell that can be vectorised.

There is an obvious trade-off between patch size n —the bigger n , the lower the spacetime’s administration overhead and the higher the impact of classic stencil optimisation techniques and vectorisation—and degree of freedom per accuracy. In [60] we apply a technique along the lines of (2) to our patches: Whenever we identify an assembly of 3×3 patches on a level ℓ , we can replace this patch by one $3n \times 3n$ patch embedded into level $\ell - 1$. The argument applies recursively. Our spacetime’s multilevel nature thus allows us to use tiny patches with Finite Volume kernels that cannot optimise too aggressively. These patches are (temporarily, as long as refinement criteria allow us to do so) replaced by larger patches on coarser tree levels. For these, optimised kernels can be written. Once an adaptivity criterion requires us to refine, we first break up the fused patches, and then continue with classic block-structured AMR with tiny patches. This technique can be read as a predecessor to the present paper’s optimisations in Section 5.

Particle-grid data structures for Particle-in-Cell, the discrete element method and SPH Lagrangian methods and particle models often employ meshes as helper data structure to speed up operations such as collision detection or the evaluation of formula which are subject to a cut-off radius. In [63], we derive a multiscale particle administration algorithm that scales. This algorithm is used for an SPH application in [21] and as base of a discrete element method code in [39] (Figure 3).

Both codes exploit the fact that each particle has a cut-off radius or a neighbourhood where we have to search for possible collisions, respectively. Both quantities determine a mesh size h if we embed the objects into a grid. Given a certain nonstationary particle distribution, we create a spacetime that can accommodate the particles: it refined down to the finest mesh size h , but particles are embedded into the level that suits their cut-off/search radius. To store them, each vertex is given a pointer to particles. Each particle is stored to the vertex on the respective level next to its centre. The efficient on-the-fly administration of

the respective particle lists is subject of discussion in [63]. On one level, we compare particles to each other within `enterCell`. Inter-grid operators in return compare particles living on various scales.

D Rationale of experimental setups

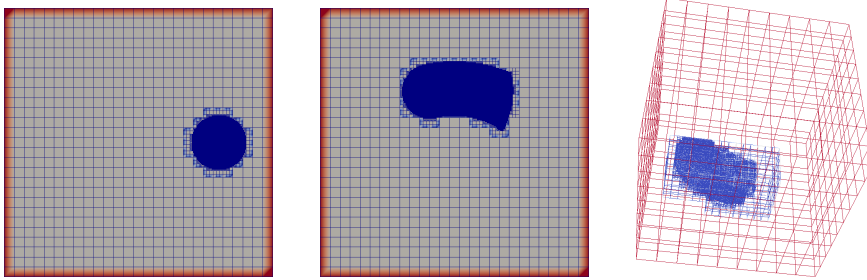


Figure 17: Grid snapshots of our $d = 2$ test setup at startup (left) and after few time steps (middle) with $h_{max} = 3^{-4}$ and $h_{min} = 3^{-8}$. The circular region of refinement runs anticlockwise. Right: Latter situation for $d = 3$ mesh with $h_{max} = 3^{-3}$ and $h_{min} = 3^{-6}$.

Throughout our experiments working with grids illustrated in Figure D we use six Peano instances holding 2, 11, 28, 768, 2,304 or 3,864 doubles per vertex or cell, respectively, where we can run 1, 2, 4, \dots , 1024 floating point operations (FLOPS) per double. For 1 and 2 FLOPS per double, our arithmetic load mirrors the Stream SCALE/Stream TRIAD benchmark [41]. Other work-per-byte configurations resemble characteristic application profiles: Two unknowns per vertex have to be stored at least for any matrix-free equation system solve. They hold the right-hand side and the solution which yields between 32 and 128 flops per double for a cell-wise matrix-vector product. If we store low-order discretisation stencils per vertex, the memory footprint grows to at least 11 doubles per vertex (9 for the stencil for $d = 2$ plus the two unknowns) or 28 for $d = 3$ if we have an analytic right-hand side. Patches within the spacetree can yield any memory footprint per grid entity, but 768 unknowns per cell or vertex, respectively, are a reasonable “small” count. It arises for example from the shallow water code [60] with 16×16 patches and three unknowns (velocity plus water height). Lattice Boltzmann with D2Q9 using 16×16 subgrids at the same time yields 2304 unknowns, while D3Q19 yields 3864 [44].

Thanks

Thanks are due to all the scientists and students who contributed to the software in terms of software fragments, applications, extensions and critical remarks. Notably, thanks are due to Hans-Joachim Bungartz and his group at Technische Universität München who provided the longest-term environment for the development of this code and Christoph Zenger who came up with the fundamental ideas concerning the space-filling curve and the usage of a stack-based automaton.

References

- [1] M. ADAMS, P. COLELLA, D. T. GRAVES, J. JOHNSON, N. KEEN, T. J. LIGOCKI, D. F. MARTIN, P. MCCORQUODALE, D. MODIANO, P. SCHWARTZ, T. STERNBERG, AND B. V. STRAALLEN, *Chombo - software for adaptive solutions of partial differential equations*, 2016. Chombo Software Package for AMR Applications - Design Document, Lawrence Berkeley National Laboratory Technical Report LBNL-6616E.

- [2] M. F. ADAMS, J. BROWN, M. KNEPLEY, AND R. SAMTANEY, *Segmental refinement: A multigrid technique for data locality*, SIAM Journal on Scientific Computing, (2016). accepted.
- [3] V. AKCELIK, J. BIELAK, G. BIROS, I. EPANOMERITAKIS, A. FERNANDEZ, O. GHATTAS, E. J. KIM, J. LOPEZ, D. O'HALLARON, T. TU, AND J. URBANIC, *High resolution forward and inverse earthquake modeling on terascale computers*, in Proceedings of the 2003 ACM/IEEE conference on Supercomputing, SC '03, New York, NY, USA, 2003, ACM.
- [4] M. BADER, *Space-Filling Curves - An Introduction with Applications in Scientific Computing*, vol. 9 of Texts in Computational Science and Engineering, Springer-Verlag, 2013.
- [5] M. BADER, M. DUMBSER, A. GABRIEL, H. IGEL, L. REZZOLLA, AND T. WEINZIERL, *ExaHyPE—an Exascale Hyperbolic PDE solver Engine*, 2015.
- [6] S. BALAY, S. ABHYANKAR, ET AL., *PETSc Web page*, 2016.
- [7] W. BANGERTH, C. BURSTEDDE, T. HEISTER, AND M. KRONBICHLER, *Algorithms and data structures for massively parallel generic adaptive finite element codes*, ACM Trans. Math. Softw., 38 (2011).
- [8] W. BANGERTH, D. DAVYDOV, T. HEISTER, L. HELTAI, G. KANSCHAT, M. KRONBICHLER, M. MAIER, B. TURCK SIN, AND D. WELLS, *The deal.II library, version 8.4*, Journal of Numerical Mathematics, 24 (2016).
- [9] W. BANGERTH, R. HARTMANN, AND G. KANSCHAT, *deal.II — a general-purpose object-oriented finite element library*, ACM Trans. Math. Softw., 33 (2007).
- [10] P. BASTIAN, M. BLATT, A. DEDNER, C. ENGWER, R. KLÖFKORN, M. OHLBERGER, AND O. SANDER, *A Generic Grid Interface for Parallel and Adaptive Scientific Computing. Part I: Abstract Framework*, Computing, 82 (2008), pp. 103–119.
- [11] ———, *A Generic Grid Interface for Parallel and Adaptive Scientific Computing. Part II: Implementation and Tests in DUNE*, Computing, 82 (2008), pp. 121–138.
- [12] R. BELLMAN, *Adaptive Control Processes: A Guided Tour*, Princeton University Press, 1961.
- [13] H.-J. BUNGARTZ, W. ECKHARDT, T. WEINZIERL, AND C. ZENGER, *A Precompiler to Reduce the Memory Footprint of Multiscale PDE Solvers in C++*, FGCS, 26 (2010), pp. 175–182.
- [14] H.-J. BUNGARTZ, B. GATZHAMMER, M. LIEB, M. MEHL, AND T. NECKEL, *Towards multi-phase flow simulations in the pde framework peano*, Comput. Mech., 48 (2011), pp. 365–376.
- [15] H.-J. BUNGARTZ, M. MEHL, T. NECKEL, AND T. WEINZIERL, *The pde framework peano applied to fluid dynamics: an efficient implementation of a parallel multiscale fluid dynamics solver on octree-like adaptive cartesian grids*, Comput. Mech., 46 (2010), pp. 103–114.
- [16] H.-J. BUNGARTZ, M. MEHL, AND T. WEINZIERL, *A parallel adaptive cartesian pde solver using space-filling curves*, in Euro-Par 2006, W. E. Nagel, W. V. Walter, and W. Lehner, eds., vol. 4128 of LNCS, Berlin, Heidelberg, 2006, Springer-Verlag, pp. 1064–1074.
- [17] H.-J. BUNGARTZ, M. MEHL, T. WEINZIERL, AND W. ECKHARDT, *Dastgen - a data structure generator for parallel c++ hpc software*, in ICCS 2008: Advancing Science through Computation, Part III, M. Bubak, G. D. van Albada, P. M. A. Sloot, and J. Dongarra, eds., vol. 5103 of LNCS, Heidelberg, Berlin, June 2008, Springer-Verlag, pp. 213–222.

- [18] C. BURSTEDDE, L. C. WILCOX, AND O. GHATTAS, *p4est: Scalable algorithms for parallel adaptive mesh refinement on forests of octrees*, SIAM J. Sci. Comput., 33 (2011), pp. 1103–1133.
- [19] E. CHARRIER AND T. WEINZIERL, *Autotuning of adaptive mesh refinement pde solvers on shared memory architectures*, in Lecture Notes in Computer Science: PPAM 2017, R. Wyrzykowski et al., eds., 2017. (accepted).
- [20] J. D. DE ST. GERMAIN, J. MCCORQUODALE, S. G. PARKER, AND C. R. JOHNSON, *Uintah: a massively parallel problem solving environment*, The Ninth International Symposium on High-Performance Distributed Computing, (2000), pp. 33–41.
- [21] W. ECKHARDT, R. GLAS, D. KORZH, S. WALLNER, AND T. WEINZIERL, *On-the-fly memory compression for multibody algorithms*, in Adv. in Parallel Comput., vol. 27, 2015, pp. 421–430.
- [22] W. ECKHARDT AND T. WEINZIERL, *A Blocking Strategy on Multicore Architectures for Dynamically Adaptive PDE Solvers*, in Parallel Processing and Applied Mathematics, PPAM 2009, R. Wyrzykowski, J. Dongarra, K. Karczewski, and J. Wasniewski, eds., vol. 6068 of LNCS, Springer-Verlag, 2010, pp. 567–575.
- [23] C. FEICHTINGER, S. DONATH, H. KÖSTLER, J. GÖTZ, AND U. RÜDE, *WaLBerla: HPC software design for computational engineering simulations*, J. Comput. Sci., 2 (2011), pp. 105–112.
- [24] G. B. GADESCHI, L. SCHNEIDERS, M. MEINKE, AND W. SCHRÖDER, *A numerical method formultiphysics simulations based on hierarchical cartesian grids*, J. Fluid Science and Technology, 10 (2015), pp. JFST0002–JFST0002.
- [25] E. GAMMA, R. HELM, R. E. JOHNSON, AND J. VLISSIDES, *Design Patterns - Elements of Reusable Object-Oriented Software*, Addison-Wesley Longman, 1st ed., 1994.
- [26] C. GOTSMAN AND M. LINDENBAUM, *On the metric properties of discrete space-filling curves*, IEEE Transactions on Image Processing, 5 (1996), pp. 794–797.
- [27] M. GRANDIN, *Data structures and algorithms for high-dimensional structured adaptive mesh refinement*, Advances in Engineering Software, 82 (2015), pp. 75–86.
- [28] M. GRANDIN AND S. HOLMGREN, *Parallel data structures and algorithms for high-dimensional structured adaptive mesh refinement*, Tech. Rep. 20, Uppsala Universitet, 2014.
- [29] M. GRIEBEL AND G. ZUMBUSCH, *Hash-storage techniques for adaptive multilevel solvers and their domain decomposition parallelization*, in Proceedings of Domain Decomposition Methods 10, DD10, vol. 218 of Contemporary Mathematics, 1998, pp. 279–286.
- [30] ———, *Parallel Multigrid in an Adaptive PDE Solver Based on Hashing and Space-filling Curves*, Parallel Comput., 25 (1999), pp. 827–843.
- [31] H. HAVERKORT, *How many three-dimensional hilbert curves are there?*, arXiv:1610.00155, (2016).
- [32] J. HUNGERSHÖFER AND J. WIERUM, *On the quality of partitions based on space-filling curves*, in International Conference on Computational Science 2002, vol. 2331 of LNCS, 2002, pp. 31–45.
- [33] T. ISAAC, C. BURSTEDDE, AND O. GHATTAS, *Low-cost parallel algorithms for 2:1 octree balance*, in IEEE 26th International Parallel and Distributed Processing Symposium, 2012, pp. 426–437.
- [34] J.-H. JEONG, N. GOLDENFELD, AND J. A. DANTZIG, *Phase field model for three-dimensional dendritic growth with fluid flow*, Phys. Rev. E, 64 (2001), p. 041602.

- [35] A. KHOKHLOV, *Fully threaded tree algorithms for adaptive refinement fluid dynamics simulations*, Journal of Computational Physics, 143 (1998), pp. 519–543.
- [36] D. E. KNUTH, *The genesis of attribute grammars*, in WAGA: Proceedings of the international conference on Attribute grammars and their applications, P. Deransart and M. Jourdan, eds., Springer-Verlag, 1990, pp. 1–12.
- [37] V. KOLOBOV AND R. ARSLANBEKOV, *Electrostatic pic with adaptive cartesian mesh*, Journal of Physics: Conference Series, 719 (2016), p. 012020.
- [38] M. KOWARSCHIK AND C. WEISS, *An Overview of Cache Optimization Techniques and Cache-Aware Numerical Algorithms*, in Algorithms for Memory Hierarchies 2002, U. Meyer, P. Sanders, and J. F. Sibeyn, eds., Springer-Verlag, 2003, pp. 213–232.
- [39] K. KRESTENITIS, T. WEINZIERL, AND T. KOZIARA, *Fast DEM collision checks on multicore nodes*, in Lecture Notes in Computer Science: PPAM 2017, R. Wyrzykowski et al., eds., 2017. (accepted).
- [40] I. LASHUK, A. CHANDRAMOWLISHWARAN, H. LANGSTON, T.-A. NGUYEN, R. SAMPATH, A. SHRINGARPURE, R. VUDUC, L. YING, D. ZORIN, AND G. BIROS, *A massively parallel adaptive fast multipole method on heterogeneous architectures*, Communications of the ACM, 55 (2012), pp. 101–109.
- [41] J. MCCALPIN, *Memory bandwidth and machine balance in current high performance computers*, IEEE Computer Society Technical Committee on Computer Architecture (TCCA) Newsletter, (1995), pp. 19–25.
- [42] M. MEHL, T. WEINZIERL, AND C. ZENGER, *A cache-oblivious self-adaptive full multigrid method*, Numerical Linear Algebra with Applications, 13 (2006), pp. 275–291.
- [43] O. MEISTER, K. RAHNEMA, AND M. BADER, *A software concept for cache-efficient simulation on dynamically adaptive structured triangular grids*, vol. 22 of Adv. in Parallel Comput., ParCo 2012, IOS Press, 2012, pp. 251–260.
- [44] P. NEUMANN, *Hybrid Multiscale Simulation Approaches For Micro- and Nanoflows*, Verlag Dr. Hut, München, 2013.
- [45] S. REITER, A. VOGEL, I. HEPPNER, M. RUPP, AND G. WITTUM, *A massively parallel geometric multigrid solver on hierarchically distributed grids*, Comput. Vis. Sci., 16 (2013), pp. 151–164.
- [46] B. REPS AND T. WEINZIERL, *A complex additive geometric multigrid solver for the helmholtz equations on spacetimes*, ACM Trans. Math. Softw., (2017). (accepted).
- [47] R. N. ROBEY, D. NICHOLAEFF, AND R. B. ROBEY, *Hash-based algorithms for discretized data*, SIAM J. Sci. Comput., 35 (2013).
- [48] R. S. SAMPATH, S. S. ADAVANI, H. SUNDAR, I. LASHUK, AND G. BIROS, *Dendro: Parallel algorithms for multigrid and amr methods on 2:1 balanced octrees*, in Proceedings of the 2008 ACM/IEEE Conference on Supercomputing, IEEE Press, 2008, pp. 18:1–18:12.
- [49] M. SCHREIBER, T. WEINZIERL, AND H.-J. BUNGARTZ, *Cluster optimization and parallelization of simulations with dynamically adaptive grids*, in Euro-Par 2013, F. Wolf, B. Mohr, and D. an Mey, eds., vol. 8097 of LNCS, Berlin Heidelberg, 2013, Springer-Verlag, pp. 484–496.
- [50] ———, *SFC-based Communication Metadata Encoding for Adaptive Mesh refinement*, in Adv. in Parallel Comput., M. Bader, ed., vol. 25, 2013, pp. 233–242.

- [51] H. SUNDAR, G. BIROS, C. BURSTEDDE, J. RUDI, O. GHATTAS, AND G. STADLER, *Parallel geometric-algebraic multigrid on unstructured forests of octrees*, in Proceedings of the International Conference on High Performance Computing, Networking, Storage and Analysis, SC '12, Los Alamitos, CA, USA, 2012, IEEE Computer Society Press, pp. 43:1–43:11.
- [52] H. SUNDAR AND O. GHATTAS, *A nested partitioning algorithm for adaptive meshes on heterogeneous clusters*, vol. 2015-June, Association for Computing Machinery, 2015, pp. 319–328.
- [53] H. SUNDAR, R. S. SAMPATH, AND G. BIROS, *Bottom-up construction and 2:1 balance refinement of linear octrees in parallel*, SIAM J. Sci. Comput., 30 (2008), pp. 2675–2708.
- [54] R. E. SWEET, *The mesa programming environment*, SIGPLAN Not., 20 (1985), pp. 216–229.
- [55] J. TEUNISSEN AND U. EBERT, *Afivo: a framework for quadtree/octree amr with shared-memory parallelization and geometric multigrid methods*, tech. rep., 2017. arXiv:1701.04329.
- [56] R. TUMBLIN, P. AHRENS, S. HARTSE, AND R. W. ROBEY, *Parallel compact hash algorithms for computational meshes*, SIAM J. Sci. Comput., 37 (2015), pp. 31–53.
- [57] J. WEINBUB, K. RUPP, AND S. SELBERHERR, *Highly flexible and reusable finite element simulations with viennax*, J. Comput. Appl. Math., 270 (2014), pp. 484–495.
- [58] M. WEINZIERL AND T. WEINZIERL, *Algebraic-geometric matrix-free multigrid on dynamically adaptive Cartesian meshes*, ACM Trans. Math. Softw., (2017). (submitted;arXiv:1607.00648).
- [59] T. WEINZIERL, *A Framework for Parallel PDE Solvers on Multiscale Adaptive Cartesian Grids*, Verlag Dr. Hut, 2009.
- [60] T. WEINZIERL, M. BADER, K. UNTERWEGER, AND R. WITTMANN, *Block fusion on dynamically adaptive spacetree grids for shallow water waves*, Parallel Processing Letters, 24 (2014).
- [61] T. WEINZIERL ET AL., *Peano—a Framework for PDE Solvers on Spacetree Grids*, 2015.
- [62] T. WEINZIERL AND M. MEHL, *Peano – A Traversal and Storage Scheme for Octree-Like Adaptive Cartesian Multiscale Grids*, SIAM J. Sci. Comput., 33 (2011), pp. 2732–2760.
- [63] T. WEINZIERL, B. VERLEYE, P. HENRI, AND D. ROOSE, *Two particle-in-grid realisations on spacetrees*, Parallel Comput., 52 (2016), pp. 42–64.